REPORT DOCUMENTATION PAGE

1. REPORT DATE (DD-MM-YYYY)	2. REPORT TYPE	3. DATES COVERED (From - To)
31-03-2006	Final	01-02-2003 To 31-12-2005

4. TITLE AND SUBTITLE
Global Instability and Control of Low Pressure Turbine Flows

5a. CONTRACT NUMBER

5b. GRANT NUMBER
F49620-03-1-0295

5c. PROGRAM ELEMENT NUMBER

6. AUTHOR(S)
Vassilios Theofilis

Nadir Abdessemed

Spencer Sherwin

5d. PROJECT NUMBER

5e. TASK NUMBER

5f. WORK UNIT NUMBER

7. PERFORMING ORGANIZATION NAME(S) AND ADDRESS(ES)

Nu Modelling, S. L.
Calle Mariano Barbacid No 1
Door 9
E-28660 Boadilla del Monte
(Madrid) Spain

8. PERFORMING ORGANIZATION REPORT NUMBER

9. SPONSORING / MONITORING AGENCY NAME(S) AND ADDRESS(ES)
Air Force Office of Scientific Research
875 N. Randolph St., Ste 325
Arlington, VA 22203-1768
Dr Jeffries / NA

10. SPONSOR/MONITOR'S ACRONYM(S)

AFRL-SR-AR-TR-06-0303

12. DISTRIBUTION / AVAILABILITY STATEMENT

DISTRIBUTION STATEMENT A. Approved for public release; distribution is unlimited.

13. SUPPLEMENTARY NOTES

14. ABSTRACT
This final report covers the 35-month period from Ferbuary 1, 2003, the inception of the grant, to its end on December 31, 2005. Within the present effort BiGlobal primary and secondary (Floquet) instability analyses of Low Pressure Turbine (LPT) flows were performed for the first time. The T-106/300 LPT blade was selected and used for the analyses reported herein. In addition, two- and three-dimensional direct numerical simulations (DNS) were employed respectively in order to provide the nonparallel steady and unsteady two-dimensional basic flows to be analyzed and in order to cross-validate primary and secondary BiGlobal instability analysis results. Calculations were performed at chord Reynolds numbers of 900 and 5000 using both structured and unstructured grids. Finally, the first-ever transient-growth analysis of a nonparallel flow field was performed in the context of the LPT flow investigated herein. In the entire range investigated, unstable three-dimensional modes were discovered; as the three-dimensional flow approaches the two-dimensional limit, the time-periodic basic state is recovered.

15. SUBJECT TERMS
BiGlobal Instability, Low Pressure Turbine Flows, Floquet theory, Transient Growth

16. SECURITY CLASSIFICATION OF: UNCLASSIFIED			17. LIMITATION OF ABSTRACT	18. NUMBER OF PAGES	19a. NAME OF RESPONSIBLE PERSON Vassilis Theofilis
a. REPORT	b. ABSTRACT	c. THIS PAGE		49	19b. TELEPHONE NUMBER (include area code) 011-34-91-336-3291

FINAL REPORT

Global instability and control of low-pressure turbine flows

Principal Investigator:
Vassilis Theofilis, Ph. D.
Numerical Modelling, S.L. Mariano Barbacid No 1, Door 9,
E-28660 Boadilla del Monte (Madrid), Spain
Voice +34 627 915 423, Fax +34 91 336 3295
E-mail, vassilis@aero.upm.es

Collaborating Investigators:
Nadir Abdessemed, M. Sc., Spencer J. Sherwin, Ph. D.
Department of Aeronautics, Imperial College London
Prince Consort Rd. London SW7 2AZ, UK

This document is the final report on research activities sponsored by the Air Force Office of Scientific Research, Air Force Material Command, USAF, under Grant number F49620-03-1-0295, entitled "Global instability and control of low-pressure turbine flows". The Grant was initially monitored by Dr. Thomas Beutner (now at DARPA) and subsequently by Lt. Col. Dr. Rhett Jefferies of AFOSR. The present report covers the 35-month period from Ferbuary 1, 2003, the inception of the grant, to its end on December 31, 2005. Within the present effort BiGlobal primary and secondary (Floquet) instability analyses of Low Pressure Turbine (LPT) flows has been performed for the first time. In addition, two- and three-dimensional direct numerical simulations were employed, respectively in order to provide the nonparallel steady and unsteady two-dimensional basic flows to be analyzed and in order to cross-validate primary and secondary BiGlobal instability analysis results. Finally, the first-ever transient-growth analysis of a nonparallel flow field has been performed in the context of the LPT flow investigated herein. The "European" T-106/300 LPT blade has been selected and used for the analyses reported herein; the relevant geometry was made available to the project by courtesy of Rolls-Royce Deutschland. I certify that there were no subject inventions to declare during the performance of this Grant. The U.S. Government is authorized to reproduce and distribute reprints for Government purpose notwithstanding any copyright notation thereon. The views and conclusions contained herein are those of the author and should not be interpreted as necessarily representing the official policies or endorsements, either expressed or implied, of the Air Force Office of Scientific Research or the U.S. Government.

CONTENTS

I.   EXECUTIVE SUMMARY

The objective of the research in the framework of the concluded Grant has been investigation of instability mechanisms active in a Low Pressure Turbine (LPT) passage, with a view of utilizing such mechanisms for flow control. To this end, the T-106/300 blade was considered, with periodic boundary conditions imposed, as appropriate, in order to simulate instability mechanisms in the entire cascade. Short of using three-dimensional DNS in order to study the phenomena involved, three classes of state-of-the-art instability computations were performed; all three have been worldwide-first applications of the respective theories to the LPT instability problem. The common challenge in all computations has been the accurate description of the reasonably complex object geometry, which prohibits reduction of the computing cost by exploitation of symmetries in the resulting flowfields. Spectral/hp element methods were used in order to meet this challenge, since these methods combine the essential for stability computations high-order (spectral) accuracy with the flexibility of unstructured methods that permits straightforward description of the complex geometry.

In the first class of computations, primary two- and three-dimensional BiGlobal instability analyses of the steady two-dimensional basic state, prevalent in the LPT flow at low chord Reynolds numbers ($Re < 1000$), have identified the character of the primary bifurcation. In a manner analogous with the prototype bluff-body cylinder flow, the two-dimensional steady basic state at the LPT flow becomes unsteady via linear amplification of its least-damped two-dimensional BiGlobal "wake" eigenmode, the latter identified herein. Three-dimensional BiGlobal analyses in this context demonstrated that all three-dimensional BiGlobal eigenmodes are stronger damped than the aforementioned (Hopf) mode. However, the same 3D analyses have revealed the existence of another, "bubble" mode which connects global instability in the trailing edge of the LPT blade with instability mechanisms in the passage wake.

The results of the first set of computations made use of a second class of analysis methodologies necessary, namely secondary (Floquet) BiGlobal instability theory. Here too, the complex geometry considered situates the present work in the forefront of presently tractable problems. The time-periodic basic state established past the primary Hopf bifurcation has been analyzed with respect to three-dimensional secondary perturbations. Unstable 3D Floquet modes were found to exist in the entire Reynolds number range investigated, $Re \in [900, 5000]$. Interestingly, the instability characteristics of the unstable Floquet modes become an ever-weaker function of the Reynolds number as the latter increases, such that the underlying physical mechanisms may be relevant to Reynolds numbers of $O(10^4)$. Furthermore, the Floquet eigenmodes are phase-locked with the basic flow, such that the only means of identifying them in the unsteady flow past the first Hopf bifurcation is the three-dimensionalization of the two-dimensional wake, resulting from their amplification. In a manner analogous to the results of the previous class of analysis, short-spanwise-wavelength Floquet modes have been identified, which connect global instability in the trailing-edge separated flow region on the blade with instability mechanisms in the wake. Both phenomena on the LPT blade, in conjunction with the analogous ones on the NACA-0012 airfoil at an angle of attack and the adverse-pressure-gradient flat-plate separation bubble, permit forming a rather consistent picture of global instability of separated flow; this has been one of the most interesting results of the present investigations. The BiGlobal analysis results of both steady- and time-periodic flows have been confirmed by three-dimensional DNS computations, also performed in the framework of this Grant.

The third class of instability analyses performed in has delivered the first-ever transient-growth (TG) results in a nonparallel flow field. The bubble-mode LPT flow instability identified by the previous methodologies was shown to support strong energy growth, a result independently obtained and cross-verified in pseudospectra analysis and three-dimensional DNS. Consequently, an alternative path to transition has been identified in the LPT flow to result from algebraic (rather than exponential) growth of small-amplitude, essentially linear, perturbations. This result opens up a whole new avenue of previously unexplored (or not recognized as such) physical mechanisms that underlie instability, transition and control of LPT flows, warranting further, in-depth studies focusing on TG phenomena.

List of Tables

FINAL REPORT
Grant F49620-03-1-0295 (Theofilis) – "Global instability and control of low-pressure turbine flows"

List of Figures

.
.
.
.

.
.
.
.
.
.

II. INTRODUCTION AND MOTIVATION

Our concern in the framework of this Grant has been with hydrodynamic instabilities of flow around a cascade of low-pressure turbine blades, using BiGlobal instability analysis tools. Use of this theory is essential in order to unravel global instabilities inaccessible to the classic linear local analysis that addresses parallel flows and focuses on (Kelvin-Helmholtz /Tollmien-Schlichting-type) instabilities – solutions of (one-dimensional) Orr-Sommerfeld-class of stability equations; at the design stages of the present project, the latter type of disturbances were not considered to be of prime relevance in the problem at hand (Rivir, personal communication). It has also been shown that BiGlobal theory is capable of recovering results of the local stability analysis, without the need to resort to the restrictive assumptions of the latter (Simens, González, Theofilis, Gómez-Blanco 2004). In addition, BiGlobal analysis has been demonstrated to be relevant to bluff body instabilities (Barkley and Henderson 1996; Theofilis, Barkley and Sherwin 2002), as well as to partial features of the flowfield at hand, such as the trailing-edge separation and its potential global instability (Theofilis 1999; Theofilis, Hein and Dallmann 2000). Finally, the significance of BiGlobal instability analysis to reduced-order modeling and flow control has been discussed extensively by Collis, Joslin, Seifert and Theofilis (2004) and further quantified recently by Noack, Tadmor, and Morzynski (2004).

Motivation for the first application of BiGlobal theory to the problem at hand was provided by the success of the theory in shedding new light on one particular (and very relevant) aspect of flow instability on a turbine blade, namely flow separation. Indeed, at the beginning of the project the potential of a laminar separation bubble to become self-excited through BiGlobal linear instability, besides being susceptible to the well-known (Kelvin-Helmholz/Tollmien-Schlichting) mechanism of linear amplification of incoming disturbances, had been recognized, both in the adverse-pressure gradient separation bubble on a flat plate (Theofilis 1999; Theofilis et al. 2000), and at the trailing-edge of a NACA 0012 airfoil at an angle of attack (Theofilis et al. 2002). These two applications are discussed in some detail next.

In the flat-plate, Hammond and Redekopp (1998) had considered a model separation bubble and, assuming quasi-parallel flow, applied linear local analysis based on numerical solutions of one-dimensional eigenvalue problems (EVP) of the Orr-Sommerfeld class in order to determine the conditions for absolute instability (Chomaz 2005) of the separation bubble. By contrast, Theofilis (1999) and Theofilis et al. (2000) had performed two-dimensional direct numerical simulations (DNS) in order to recover the separated-bubble boundary-layer flows described by Briley (1971) and used such (essentially nonparallel) 2D steady flows as basic states in 3D BiGlobal linear instability analyses. The appropriate (partial-differential-equation-based) EVP was solved numerically and the potential of separated flow to support global instability, without having to resort to restrictive assumptions of a parallel/quasi-two-dimensional basic flow, was demonstrated for the first time. The agreement between one conjectured scenario of topological changes in the reattachment zone of a laminar separation bubble on account of BiGlobal instability, alongside the associated necessary wall-shear distribution (Dallmann, Vollmers, Su and Zhang 1997), on the one hand, and the computed wall-shear distribution ensuing instability of the first (stationary) unstable BiGlobal eigenmode of the Briley bubble, on the other, is shown in Figure 1 (Theofilis et al. 2000). The scenario discovered points out that vortex shedding from bluff bodies may be recovered (possibly amongst other mechanisms) by linear amplification of three-dimensional BiGlobal eigenmodes.

Theofilis and Sherwin (2001) extended this work to detect BiGlobal eigenmodes in the trailing-edge separation region of a NACA 0012 airfoil at a chord Reynolds number of $Re = 1000$ and an angle of attack $\alpha = 5°$. The grid utilized for the simulations is shown in Figure 2, while the basic flow obtained, including a magnification of the trailing-edge separation region, is also shown in the same figure, in terms of the magnitude of flow vorticity. Spectral/hp element technology (Karniadakis and Sherwin 2005) was utilized for

the first time in the context of BiGlobal analysis in this work, in order to successfully address the issues of accuracy needed in instability analyses in conjunction with the complex geometry at hand.

Figure 1: Conjectured vortex-shedding mechanism *(left)* and associated wall-shear distribution *(middle)* on account of a self-excited laminar separation bubble. *Right:* computed wall-shear distribution of the most unstable BiGlobal eigenmode superimposed upon τ_w of the Briley bubble, indicating the generation of secondary reattachment/separation/reattachment in the primary reattachment region (Theofilis, Hein and Dallmann 2000).
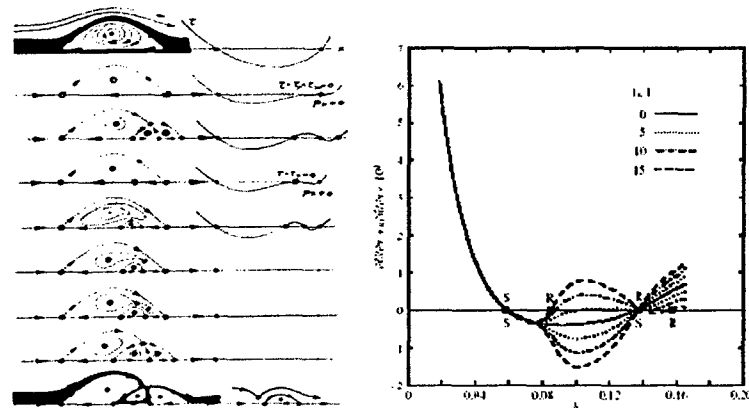
A scan of the entire spanwise domain (considered homogeneous) delivered only damped BiGlobal eigenmodes associated with the trailing-edge separation. The spatial structure of the most unstable eigenmode is reminiscent of that found in the Briley bubble (Theofilis *et al.* 2000), and is shown in terms of the magnitude of the spanwise disturbance velocity component in the left part of Figure 3. Subsequently, Theofilis *et al.* (2002) performed BiGlobal instability analysis of the entire NACA 0012 flow-field, considering an integration domain extending well into the free-stream, upstream and downstream of the airfoil; they demonstrated that the most unstable eigenmode of the flow in question, at the same parameters as those used by Theofilis and Sherwin (2001), is that in the related wake-flow, shown in the right part of Figure 3. Note that no assumptions on the form of the basic flow have been made in the analysis of Theofilis *et al.* (2002), although the near-parallel nature of the basic state in the wake might have permitted analysis based on the classic one-dimensional linear theory.

Figure 2: Unstructured grid *(left)* and extracts of the steady basic flowfield *(right)* on a NACA0012 airfoil at chord $Re = 1000$ and angle of attack $\alpha = 5°$ (Theofilis and Sherwin 2001).
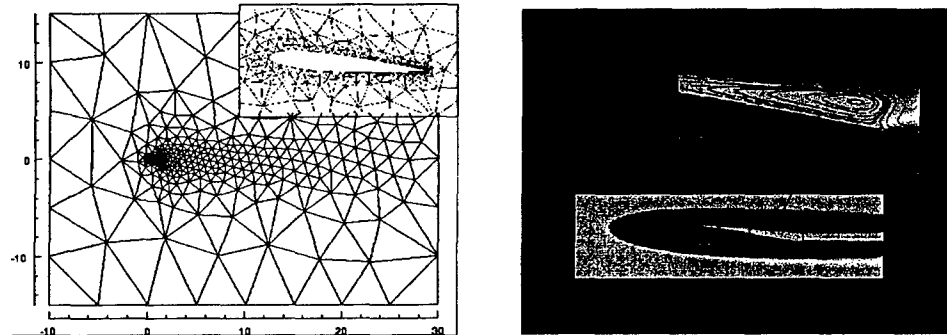
Figure 3: *Left:* The structure of the spanwise velocity component of the (least stable) BiGlobal eigenmode in the separated trailing-edge region (Theofilis and Sherwin 2001). *Right:* Magnitude of disturbance vorticity of the most unstable eigenmode of the flow, in the wake (Theofilis, Barkley and Sherwin 2002).
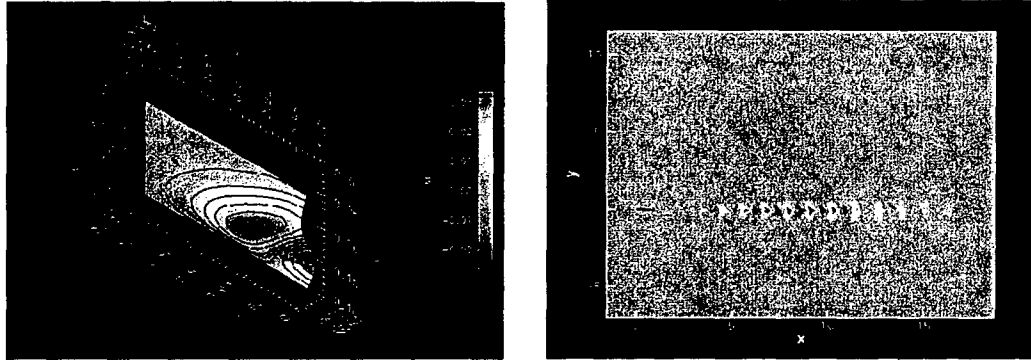
As mentioned, research in the framework of the present Grant is concerned with instability mechanisms in the flowfield around a blade model in an LPT passage. The ultimate objective of the work is to understand the physics behind the successful application of (active) flow control in experiments (Sondergaard, Rivir, Bons, and Yurchenko 2004) and three-dimensional DNS (Fasel, Gross and Postl 2003; Rizzetta and Visbal 2004), the latter modeling the actual flow around LPT blades at Reynolds numbers of $O(10^5)$. A central issue in DNS of LPT flows (e.g. Wu and Durbin 2001, Wissink 2002) is the understanding of the physical mechanisms that describe the three-dimensional nature of the instabilities in this class of flows. However, the computational effort that underlies three-dimensional DNS renders this numerical approach accessible only to large-scale facilities and certainly inappropriate for detailed parametric studies, in view of which, the alternative, more efficient for linear instability analyses, methodology based on BiGlobal theory has been chosen in the current research effort.

In the context of BiGlobal theory, a two-dimensional DNS need be performed in order for the basic state to be obtained and analysed with respect to its stability against the full range of spanwise wavenumbers at each Reynolds number value. Either the eigenvalue problem (EVP), or a Transient Growth (TG) methodology may be used; they are both linear but differ in the treatment of the time-dependence of the linearized equations. While the TG resolves the time-dependence of the linearized system as an Initial Value Problem (IVP), the EVP explicitly imposes harmonic time-dependence of the small-amplitude perturbations. However, in both cases, the two-dimensional variable coefficients of the linearized equations of motion comprise the aforementioned basic state, provided by the two-dimensional DNS. As is well-known in linear instability theory, accuracy of this basic state is a prime consideration which, in the context of the BiGlobal analysis, translates in the necessity of faithful representation of the LPT blade geometry; this, in turn, poses a challenge for numerical methods employed for the solution of both the basic flow problem and the associated BiGlobal EVP or IVP. Here, the numerical solution of the two-dimensional Navier-Stokes equations has been performed using a DNS solver based on the spectral/hp element method (Karniadakis and Sherwin 2005) and either structured or hybrid (partly structured and partly unstructured) meshes, based on quadrilateral and triangular elements, within which high-order polynomials are used in order to expand the unknowns. The subsequent instability analysis was also performed using a spectral element methodology for the spatial discretization and Krylov subspace iteration for the recovery of the most significant part of the eigenspectrum. This approach has been shown in the past to be an appropriate (as well as efficient) means to study the stability of complex flows (cf. that over a NACA0012 airfoil by Theofilis *et al.* 2002).

11

All items contemplated in the work plan of the Grant have been completed successfully. Two flavors of BiGlobal instability analysis have been followed. First, analysis of the steady two-dimensional basic flow (obtained by unsteady 2D DNS) has been performed in order to identify the first (Hopf) bifurcation of the flow from a two-dimensional steady to a two-dimensional unsteady state. Three-dimensional analysis in this context has also been performed, in order to assess the relative importance of two- and three-dimensional BiGlobal perturbations superposed upon the steady state. Second, in view of the results obtained in the first part, BiGlobal secondary theory based on Floquet secondary analysis has been performed in order to study, for the first time, instability of a *non-symmetric* nonparallel time-periodic basic state. The results permitted identification of the linear stability boundaries of the time-periodic flow, as well as distinct types of three-dimensional perturbations involved in this process. Three-dimensional DNS has confirmed the results of both aforementioned flavors of BiGlobal analysis. Finally, the first-ever BiGlobal Transient Growth (TG) analysis of a nonparallel basic state has been performed within the framework of the completed research. Its results shed additional light to the issue of linear instability of the bluff body at hand, especially in terms of algebraic growth of perturbations associated with the trailing-edge separation region. Section III presents the theoretical background necessary in order to follow the work performed in Section IV. Results are summarized in Section V, where an outlook of potential extensions of the present work is offered.

III.   THEORETICAL BACKGROUND

1. The incompressible BiGlobal eigenvalue problem (EVP)

In the course of the Grant concluded, BiGlobal instability theory was applied for the first time to low-pressure turbine flows in the incompressible regime. A review of this analysis methodology and its application to a wide spectrum of flows has been presented by Theofilis (2003). The analysis proceeds with the incompressible equations of motion into which the BiGlobal instability Ansatz, shown in Table 1, is substituted. Note that in this table single primes refer to time- or space-periodic quantities, and double primes refer to spatial coordinates with mild variation in comparison with that on the non-primed spatial coordinates. Primed quantities are modeled (as either periodic or mildly-dependent on the corresponding spatial direction) while unprimed quantities are fully resolved. According to BiGlobal theory, any flow quantity $q(x,y,z,t) = (u, v, w, p)^{\mathrm{T}}$ is decomposed into $\bar{q}$, an O(1) steady two-dimensional basic state, and $\hat{q}$, a small-amplitude, O(ε), unsteady three-dimensional perturbation. Linearization results in the complex non-symmetric generalized BiGlobal EVP

$$[\mathcal{L} - (\mathcal{D}_x\bar{u})]\hat{u} - (\mathcal{D}_y\bar{u})\hat{v} - \mathcal{D}_x\hat{p} = -i\Omega\hat{u},$$

$$-(\mathcal{D}_x\bar{v})\hat{u} + [\mathcal{L} - (\mathcal{D}_y\bar{v})]\hat{v} - \mathcal{D}_y\hat{p} = -i\Omega\hat{v},$$

$$-(\mathcal{D}_x\bar{w})\hat{u} - (\mathcal{D}_y\bar{w})\hat{v} + \mathcal{L}\hat{w} - i\beta\hat{p} = -i\Omega\hat{w},$$

$$\mathcal{D}_x\hat{u} + \mathcal{D}_y\hat{v} + i\beta\hat{w} = 0,$$

or, in compact form,

$$\mathcal{L}\,\dot{q} = \Omega\mathcal{R}\,\dot{q},$$

for the determination of the complex eigenvalue $\Omega = \Omega r + i\,\Omega i$ and the complex amplitude functions – components of the eigenvector, $\hat{q} = (\hat{u},\hat{v},\hat{w},\hat{p})^T$. Input parameter of the analysis are the flow Reynolds number, Re, a wavenumber β, associated with a spanwise periodicity length L_z through $L_z = 2\pi / \beta$, and the steady basic state $\bar{q} = (\bar{u},\bar{v},\bar{w})^T$, described by the velocity components (no base pressure is necessary) and their derivatives with respect to the spatial coordinates x and y. In the temporal framework used, $\Omega_r = Re(\Omega)$ represents the amplification/damping rate, while $\Omega_i = Im(\Omega)$ is the frequency of the disturbance sought. In view of the two-dimensional nature of the basic state, a simple transformation (Theofilis 2003) permits converting the complex EVP into a real one, thus halving the storage requirements and expediting the computations involved. The system must be closed by appropriate boundary conditions over the two-dimensional domain on which the LPT blade is defined and discretized. For the present problem these are the no-slip condition at the surface of the turbine-blade, zero disturbance velocity at the inflow and $\partial\hat{u}/\partial n = \partial\hat{v}/\partial n = 0$ at the outflow boundary, n denoting the direction normal to that boundary, as well as periodic connectivity of all flow quantities at the lower and upper boundaries, as illustrated in Figure 7 of Section IV.

13

Table 1: Linear Stability Theory Decompositions.

Theory	Basic state	Eigenmode	
		Amplitude function	Phase function
TriGlobal	$\bar{q}(x_1, x_2, x_3)$ +	$\hat{q}(x_1, x_2, x_3)$ ·	$\Theta_{3d}(t)$; $\Theta_{3d} = -\Omega t$
Parabolized Stability Equations - 3D	$\bar{q}(x_1'', x_2, x_3)$ +	$\hat{q}(x_1'', x_2, x_3)$ ·	$\Theta_{2d}''(x_1''; t)$; $\Theta_{2d}'' = \int_{x=x_0}^{x''} \alpha(\xi)\, d\xi - \Omega t$
BiGlobal Secondary Theory	$\bar{q}(x_1, x_2, x_3'; t')$ +	$\sum_{n=-\infty}^{\infty} \hat{q}(x_1, x_2, x_3', t')$ ·	$\Theta_{2d}'(t')$; $\Theta_{2d}' = \sigma t$
BiGlobal	$\bar{q}(x_1, x_2)$ +	$\hat{q}(x_1, x_2)$ ·	$\Theta_{2d}(x_3; t)$; $\Theta_{2d} = \beta x_3 - \Omega t$
Parabolized Stability Equations	$\bar{q}(x_1'', x_2)$ +	$\hat{q}(x_1'', x_2)$ ·	$\Theta_{1d}''(x_1'', x_3; t)$; $\Theta_{1d}'' = \int_{x=x_0}^{x''} \alpha(\xi)\, d\xi + \beta x_3 - \Omega t$
Herbert Secondary Theory	$\bar{q}(x_1', x_2; t')$ +	$\sum_{n=-\infty}^{\infty} \hat{q}(x_1', x_2, t')$ ·	$\Theta_{1d}'(x_3; t')$; $\Theta_{1d}' = \beta x_3 - \sigma t$
Rayleigh / Orr-Sommerfeld	$\bar{q}(x_2)$ +	$\hat{q}(x_2)$ ·	$\Theta_{1d}(x_1, x_3; t)$; $\Theta_{1d} = \alpha x_1 + \beta x_3 - \Omega t$

Regarding numerical solution of the BiGlobal eigenvalue problems, it should be noted that the matrix

$$\mathcal{C} = \mathcal{L}^{-1} \mathcal{R}$$

discretizing the EVP is never formed explicitly. Instead, the EVP can be expressed in the time-differential form

$$\partial \hat{q} / \partial t = \mathcal{C}\, \hat{q}.$$

In order to solve this equation in an efficient manner the Arnoldi algorithm, which is based on a Krylov subspace iteration method (Theofilis 2003), has been used in combination with the exponential power approach. The exponential power method solves this equation analytically

$$D\hat{q}(t) \equiv \hat{q}(t + \Delta t) = \hat{q}(t) \exp\left(\int_{t}^{t+\Delta t} C\, d\tau \right)$$

Where C discretizes $\mathcal{C}$. Employing the Arnoldi algorithm on the evolution operator $D(t)$, which evolves the field $\hat{q}$ from time t to time $t + \Delta t$ (and can be determined through a time-stepping algorithm) yields the dominant eigenvalues of $D \equiv \exp(C\Delta t)$. Since only the stability-significant leading eigenvalues are calculated, the run-time associated with the total process of building the Krylov subspace and obtaining the eigenvalues of the Hessenberg matrix constructed by the iteration is a small fraction of that required by classic methods, such as the QZ algorithm. The EVP solution algorithm then follows the path highlighted in Figure 4. The equations of motion are integrated in time for sufficient enough time in order to form the EVP shown and solve it using the iterative Arnoldi method; see Karniadakis and Sherwin (2005) for further details.

14

Figure 4: Schematic representation of the possible numerical procedures for the solution of the BiGlobal EVP. Highlighted is the option used, in which the matrix is not formed; also shown (but not used) is the case of a direct solution, via matrix storage.
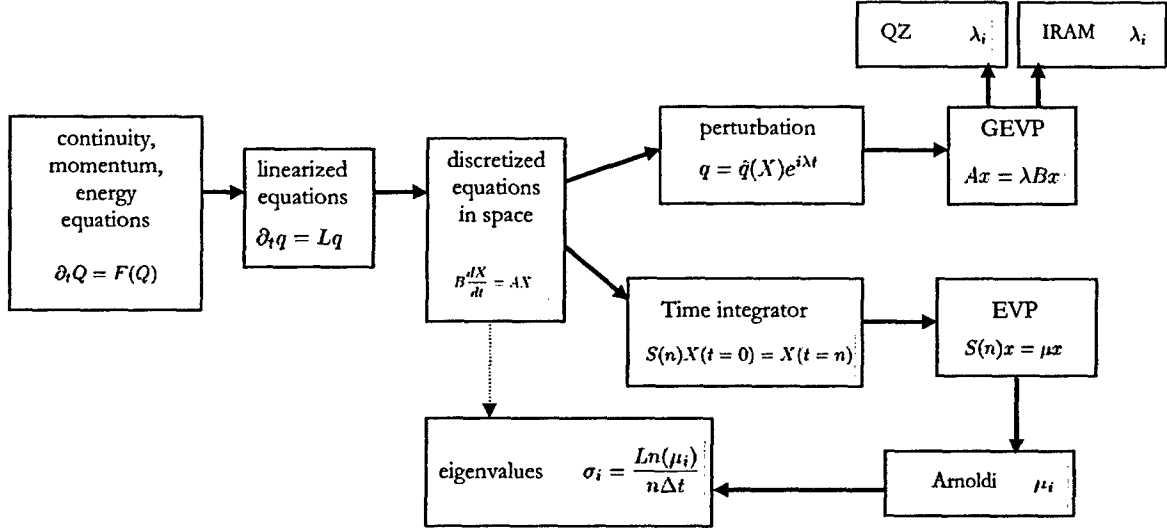
2. Floquet analysis of 3D perturbations of the time-periodic 2D flow

When the basic state to be analyzed is periodic in time, the (basic-flow-related) coefficients of the BiGlobal EVP are periodic functions of time, for which Floquet analysis is appropriate. Such a situation arises past the primary Hopf bifurcation in the LPT blade. Concretely, past the critical Reynolds number for amplification of the two-dimensional BiGlobal eigenmode, the T-periodic two-dimensional basic state takes the form $q(x, y, t) = q(x, y, t + T)$, where q is the state vector comprising two velocity components and pressure.

Its stability may be analyzed through study of the eigenvalues μ of the monodromy matrix operator M, defined as

$$M = \int_{t_0}^{t_0+T} [N(t') + L] dt'$$

where L and N respectively denote the linear and nonlinear parts of the incompressible equations of motion. The eigenvalues μ are called the Floquet multipliers. For a normalized period T, $\mu > 1$ describes a growing orbit, while $\mu < 1$ leads to a limit cycle (Tuckerman and Barkley 2000). Numerical approaches analogous to those used for the iterative solution of the BiGlobal eigenvalue problem are followed, although Floquet analysis requires the time-discretization of the periodic orbit by, say, nt snapshots within one period. In turn, the leading dimension of the matrix discretizing the BiGlobal secondary instability analysis EVP is a system of **nt coupled systems**, each of size equal with one BiGlobal EVP. As, the leading dimension of the matrix solved in Floquet analysis can easily become of $O(10^5)$; use of iterative methods for the computation of its eigenspectrum is imperative.

IV. TECHNICAL RESULTS

1. Geometry and spatial discretization

Figure 5: The T-106/300 LPT blade

The present work is concerned with linear instabilities of flow in a Low Pressure Turbine passage. The well-documented "European" T-106 LPT blade model, shown in Figure 5, has been used; its coordinates may be found in the Appendix. As a first step the spatial domain analyzed must be defined and discretized by a numerical approach appropriate for BiGlobal instability analyses. Key ingredients of such a numerical method are its high-order of accuracy (Theofilis 2003) and, in the case of the flowfield analyzed, its ability to resolve complex geometries. Furthermore, the consideration of a cascade of LPT blades, as opposed to analyzing flow around a single blade, requires imposition of periodic boundary conditions along one of the two spatial directions resolved. All three requirements naturally lead to using spectral/*hp* element methods (Karniadakis and Sherwin 2005). In short, these methods permit achieving spectral accuracy in complex geometries by offering independent control of two parameters, *h*, the degree of resolution of the domain considered, and *p*, the degree of polynomial considered in order to resolve the quantity sought within each of the elements defined in the space tessellation. Grid independence within the spectral/*hp* element method is achieved by *independently* controlling these two parameters.

The main advantage of spectral/*hp* elements over other approaches to resolve complex geometries (e.g. finite-elements) resides in the fact that, if only the number of nodes, *h*, were to be increased (*h*-refinement), as shown in Figure 6, correct description of the surface resolved and grid-independence of the results obtained would only be achievable through a progressive increase of the number of nodes utilized, up to at a large resolution, say "Mesh 6" in Figure 6, were reached. By contrast, the spectral/*hp* element method permits increase of *p* (*p*-refinement), at any level of *h*-refinement (say, "Mesh 4" in Figure 6), such that the resolution (and associated memory) requirements for convergence remain tractable, even for relatively complex geometries. These properties of the numerical approach followed have been fully exploited in the computations that follow.

16

Figure 6: Grid-independence, achieved through h-refinement.
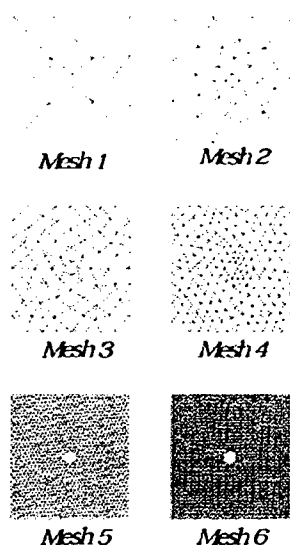
Within the framework of the spectral/hp element method both structured and unstructured spatial discretizations are possible and both approaches have been followed in the early stages of our computations, in order to gain some confidence in the numerical results produced. In both cases a single blade has been considered and inflow/outflow boundary conditions have been imposed at the West and East boundaries of the computational domain, where constant inflow and appropriate stress-free outflow conditions have been imposed. At the North and South computational boundaries of the resolved domain periodicity has been imposed; in most of the computations of both the basic flow and the subsequent instability analyses one periodicity domain has been considered.

Within a structured discretization, appropriate space tessellations have been designed, which use classical h - refinement to resolve the boundary layers and then apply a high order polynomial expansion within each subdomain. In the cases studied a $p = 8$ polynomial order expansion has been applied within each elemental domain. An example of a typical structured mesh utilized is shown in the left column of Figure 7; using the same polynomial degree as that used for the computations of flow in the domain interior avoids spuriously generated instability on account of poor surface representation. This type of technique is also possible with unstructured domains and has the advantage that the surface geometry is also represented by high order polynomial expansions. Most computations have been performed on a hybrid structured / unstructured mesh, employing the same structured strategy to resolve the immediate neighborhood of the blade, including the boundary layers, and a triangular mesh for the rest of the flow, as shown in the right column of Figure 7. Compared with the structured-, the hybrid strategy has the advantage of permitting selective resolution of critical regions in the flowfield, such as the vicinity of the tip and the wake regions of the blade. In order to further verify the integrity of results subsequently obtained, numerical experimentations have been performed, using different extents of the discretized domain and monitoring changes in basic flow and instability analysis results obtained. Specifically, the periodicity length has always been kept the same, and either the inflow- or the outflow part of the hybrid domain has been extended in a manner shown in Figure 8. In both cases, the baseline domain, denoted by "0", is the hybrid domain shown in Figure 7, in which 200 points and cubic spline interpolation between them is used to define the blade geometry and a total of 2000 elements are used to resolve the entire flowfield.

17

Figure 7: Upper row: Typical structured (left column) and hybrid (right column) spectral/hp element meshes, resolving flow around a single T-106/300 LPT blade. 200 elements and polynomial degree $p=4$ have been used for the moderate-resolution structured discretization, while 2000 and $p=8$ have been used for the hybrid discretization. In the lower row, details of the respective near-field resolution (left) and polynomials (right) are shown, including collocation points.
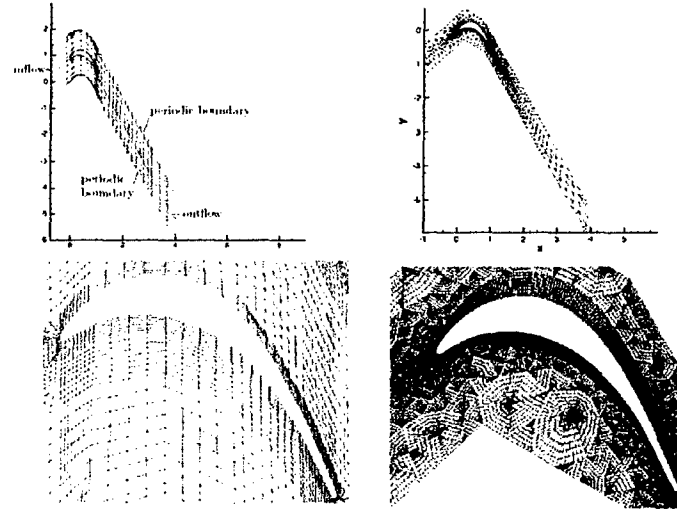
Figure 8: Extensions of the computational domain in either the inflow (left) or the outflow (right) direction, respectively keeping constant the discretization of the outflow and inflow direction.
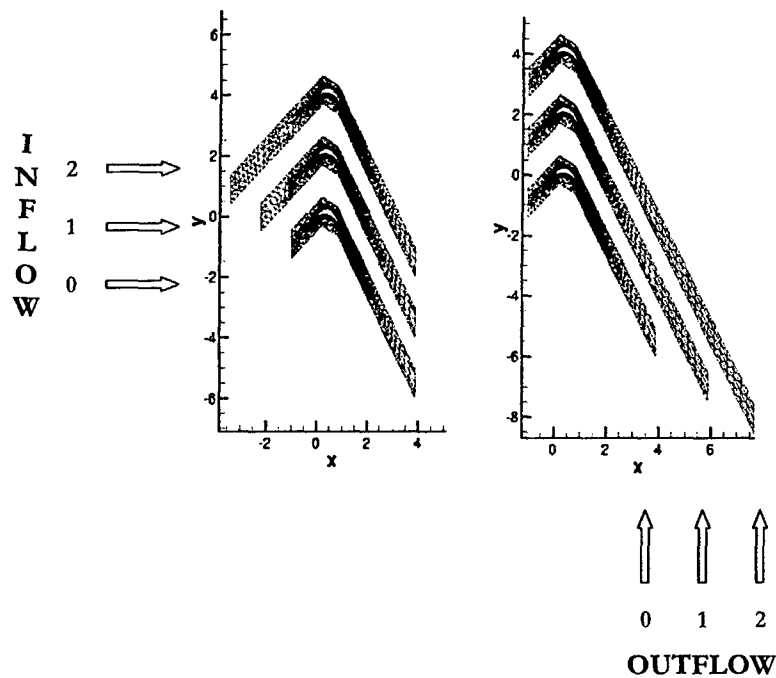
2. Basic flow computations

First, incompressible steady and time-periodic basic states have been computed numerically at several transitional chord-Reynolds numbers, $Re = U_\infty\, c\, /\, \nu$, where $U_\infty = 1$ is the inflow velocity magnitude, c is the blade chord and ν is the kinematic viscosity, to be analyzed subsequently using BiGlobal theory. In order to obtain a basic understanding of the flow and its instability characteristics in terms of the parameter range of the first two-dimensional bifurcation, initial computations were based on the less expensive structured mesh, followed by refined computations using both types of meshes. Indeed, as subsequent computations confirmed, exploratory two-dimensional DNS computations using the structured grid presented in Fig. 7 have identified the bracket within which the first 2D BiGlobal eigenmode is expected to be amplified, in the region $500 < Re < 1000$, as shown in Figure 9.

Figure 9: Spanwise vorticity in structured-, moderately-resolved computations.
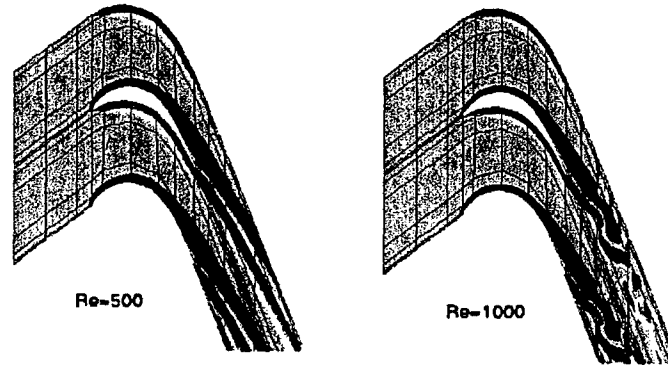
Subsequently, computations have been performed on the unstructured mesh of Fig. 7 and results obtained are shown in terms of flow vorticity in Figure 10. These results confirmed, and narrowed to $750 < Re < 1000$ the range within which the first two-dimensional bifurcation is expected. Prior to discussing this issue, though, some integral steady flow properties are presented. Fig. 10 highlights one particular feature of the basic state, on which attention has been drawn in subsequent instability analyses, namely the existence of a steady separation region in the trailing edge of the LPT blade.

Figure 10: Snapshots of the basic flow vorticity and magnification of the respective trailing-edge separation regions at chord $Re = 500, 750$ and 1000.
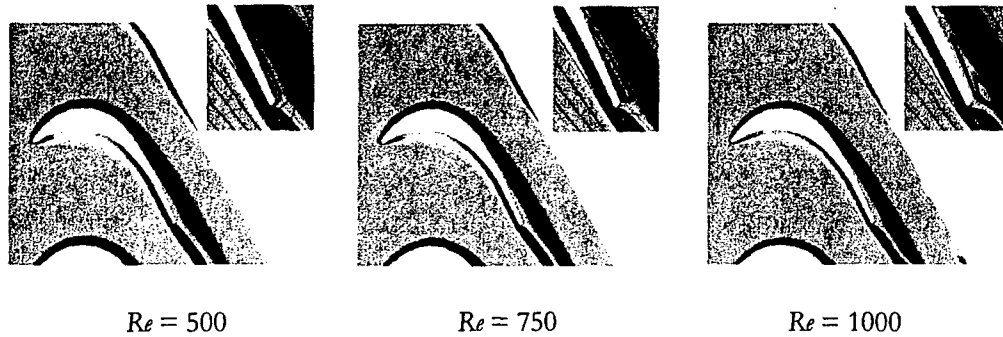
$Re = 500$ $Re = 750$ $Re = 1000$

The size of and strength of recirculation in the separation zone grows with growing Reynolds number, the latter corresponding to steady flow. Once unsteadiness has set in, the primary reattachment zone of the trailing-edge separation bubble breaks up periodically in a manner reminiscent of the vortex shedding discovered by Theofilis *et al.* (2000), as being the result of linear amplification of a three-dimensional BiGlobal eigenmode. A trailing-edge separation region was also discovered by Theofilis *et al.* (2002) on the NACA-0012 airfoil at an angle of attack, where (stable) BiGlobal eigenmodes were also identified. It was thus considered important to understand the different BiGlobal instability mechanisms operating in this region and their potential association with the generation of global instability in the LPT blade wake, as well as a possible connection of the latter to the former mechanism. In order to quantify the separation zone and relate it with known bluff-body instabilities, an equivalent bluff-body diameter, D, has been defined as the distance between the local maxima of the velocities just downstream of the trailing-edge of the LPT blade, as schematically depicted in Fig. 11. The ξ–line is taken to be tangent to the trailing edge and perpendicular to the flow direction in the downstream wake, and D is defined as

$$D = \left| \xi(\max(\overline{u}(x,y))) - \xi(\min(\overline{u}(x,y))) \right|$$

Figure 11: Definition of the equivalent bluff-body diameter, D.
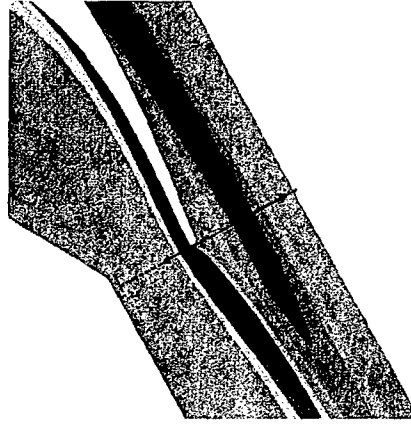
For flows close to a transitional state, $D \approx 0.3\,c$, and hence a Reynolds number based on this length is of O(300), which is significantly higher than that at which the Hopf bifurcation occurs in the (isolated) cylinder case. In order to examine the validity of this argument, two-dimensional DNS was performed for a periodic array of cylinders placed at the same distance from each other as the LPT blades under consideration. This placement did not change the O(50) critical Reynolds number for the first transition on the cylinder, which led us to attribute the large difference in Reynolds numbers associated with the Hopf bifurcation to the asymmetry of the geometry of the present blade object.

In order to complete the description of two-dimensional flow results, the pressure- and cp-distribution has been computed for different chord-based Reynolds numbers. Figure 12 shows the time-averaged pressure and pressure-coefficient distribution, which do not change qualitatively with changing Reynolds number. Interestingly, one can observe a distinct area of reduced pressure (increased suction) on the pressure surface at the very trailing edge, which results in a "kink" of the c_p-coefficient at $x/c \approx 1$. This is a result in line with the one shown by Postl, Gross and Fasel (2004) at an order-of-magnitude higher Reynolds number and has been verified to be a feature of the converged flowfield at the present parameters by means of several *h*- and *p*-refinements.

20

Figure 12: Time-averaged pressure distribution of the two-dimensional basic flow at $Re_c = 1000$. Upper: around the entire blade and in the neighborhood of the trailing edge. Lower: Pressure coefficient distribution against chord length.
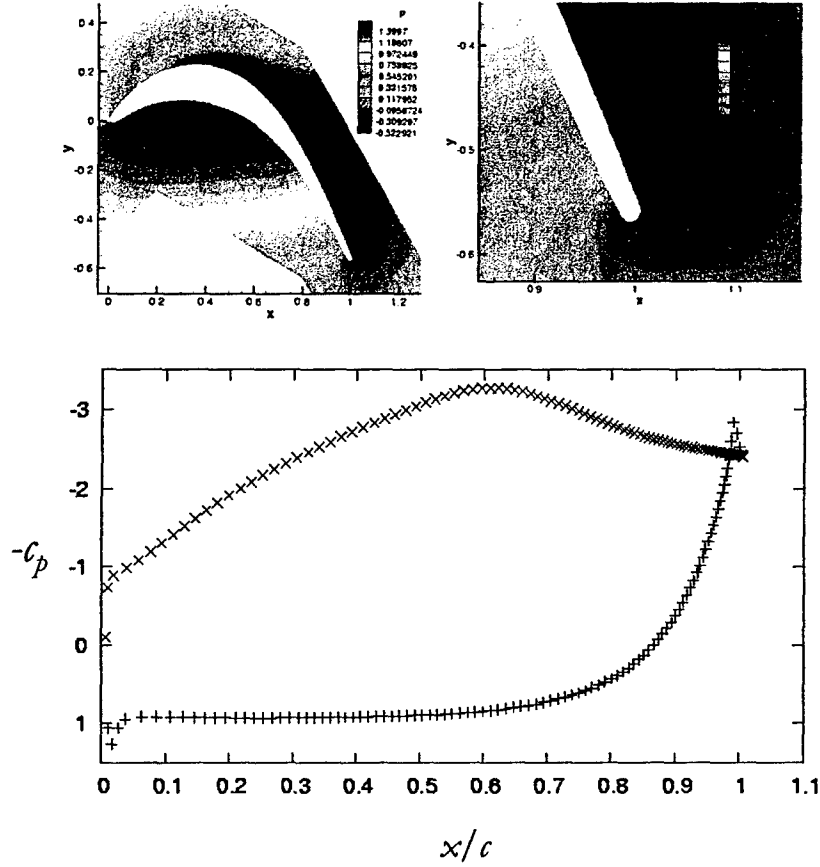
3. Three-dimensional instability analysis of two-dimensional steady basic states

There is no general rule as to whether two- or three-dimensional perturbations will be the first to be amplified, although Squire's theorem, applicable to one-dimensional profiles in incompressible flows, does provide some guidance (Drazin and Reid 1981). In the case of BiGlobal instability of nonparallel (two-dimensional) basic states evidence from a handful of analyzed flows is contradictory. As an example, while the steady state of the circular cylinder first becomes unstable to two-dimensional modes through a Hopf bifurcation and subsequently through three-dimensional instability of the ensuing time-periodic state (Barkley and Henderson 1996), the steady two-dimensional lid-driven cavity flow becomes unstable to three-dimensional disturbances prior to the onset of two-dimensional unsteadiness (Theofilis 2000; Poliashenko and Aidun 1995). In the present new problem, it is thus necessary to address linear amplification of both two- and three-dimensional BiGlobal eigenmodes; we commence the analyses with the first. In what follows, Re will be used to denote chord-based Reynolds number.

21

3.1. Identification of the critical Reynolds number for two-dimensional BiGlobal instability.

Two independent paths have been followed in order to answer the question of critical Reynolds number associated with two-dimensional ($\beta=0$) BiGlobal perturbations. First, the range identified in the previous section as containing the critical Reynolds number for the Hopf bifurcation was refined by means of the same two-dimensional DNS used for the prediction of the basic states. Second, the BiGlobal eigenvalue problem pertinent to a steady basic state at a given Reynolds number was solved for the particular case $\beta=0$. The results of the two approaches were then compared and accepted when agreement was obtained. Indirectly, this exercise defined the necessary resolution requirements for reliable results to be obtained by either of the approaches.

Starting from a low $Re = 700$, convergence of the steady basic state was obtained on an unstructured mesh and the resulting flow was analyzed with respect to two-dimensional perturbations. In the process, an h-refinement was performed, keeping the same polynomial degree $p = 7$; results are presented in Table 2. The differences in the results on the damping rate of the leading eigenvalues, as generated by the inexpensive structured and either of the unstructured meshes, is confined in the third significant; that between the well-resolved unstructured meshes is of $O(10^{-6})$.

Table 2: Variation of mesh density and its distribution versus eigenvalues for Re=700 and p=7

Element Count	Eigenvalue #	Damping rate ω_r	Frequency ω_i
224	1	-0.55793	0
	2	-1.11947	±2.08443
1586	1	-0.58996	0
	2	-1.04967	±1.70023
2028	1	-0.58996	0
	2	-1.05098	±1.70362

The high-order spectral/hp scheme has been applied using different polynomial orders p in order to investigate the correlation between the accuracy of the solution and the chosen polynomial expansion. The objective here is to employ polynomial orders of sufficient degree to describe the flow physics and yet low enough for the computations to remain efficient. Table 3 summarises results based on both the structured- and the hybrid meshes for different values of p at $Re = 870$ at approximately the same mesh count. While the structured mesh needs $p = 9$ in order to yield results accurate to within two significant figures (as compared with results at $p = 8$, not shown here), the polynomial degree necessary in order to reach convergence when using the hybrid mesh approach is lower than that required by the structured code; at these parameters, $p = 6$ yields satisfactory convergence to four significant figures. As a consequence, for all the subsequent instability analyses, the hybrid mesh strategy was followed.

Table 3: Dependence of the eigenvalue on the polynomial degree, p, at $Re = 870$.

Polynomial Order	Structured mesh		Hybrid mesh	
p	ω_r	ω_i	ω_r	ω_i
3	-0.213743	±1.69066	-0.199461	±1.63790
6	-0.218046	±1.67449	-0.187688	±1.62462
9	-0.153072	±1.58980	-0.187684	±1.62445

The final exercise performed in order to ensure accuracy of the instability results obtained herein has monitored the effect on the eigenvalues of performing the analysis in domains of different extents (on which previously the basic state has also been obtained). Specifically, the hybrid meshes of Fig. 8 were considered: they all part from the same baseline mesh, denoted as "0", resolve the neighbourhood of the blade by the same quality hybrid mesh (a feature of the unstructured-mesh generator used) and respectively extend the resolved domain by different amounts in either the upstream or downstream direction; the extent of the periodic direction remains identical in all five domains considered. Basic state computations were performed at the Reynolds number value previously analyzed, $Re = 870$ and, subsequently, BiGlobal instability analyses were performed at $\beta = 0$; the results are shown in Table 4. Since the leading eigenvalue does not change significantly with the respective changes in the extent of the resolved domain, the Baseline configuration "0" has been used for the subsequent stability analyses of steady two-dimensional basic flows.

Table 4: Dependence of the leading eigenvalue on the mesh extent at $Re = 870$

Mesh Extension	Damping rate ω_r	Frequency ω_i
Baseline – "0"	0.187688	±1.62462
Inflow "1"	0.190672	±1.63403
Inflow "2"	0.191463	±1.63627
Outflow "1"	0.187771	±1.62479
Outflow "2"	0.188251	±1.62577

As the flow comes closer to the onset of two-dimensional instability, convergence is increasingly more challenging to obtain. This is a well-known situation from other complex nonparallel flows that require BiGlobal analysis in order to identify their first Hopf bifurcation, such as that in the classic square lid-driven cavity (Poliashenko and Aidun 1995). The spatial structure of the spanwise vorticity associated with the leading damped eigenmode at two particular Reynolds numbers, $Re = 820$, and one very close to unsteadiness (but still corresponding to steady flow), $Re = 895$, is shown in Figure 13. We term this structure *wake*-mode instability, since it is associated with instability in the wake of the LPT blade. As the critical Reynolds number for amplification of two-dimensional disturbances is approached, the intensity of the wake mode increases and the amplitude function tends toward the trailing edge. The time-periodic unsteady flow patterns observed in the DNS at Reynolds numbers above $Re_{crit,2D}$ are the result of *linear* amplification of the wake mode.

Figure 14 summarises the damping rates using either the structured- or the unstructured/hybrid-mesh approaches, assuming no perturbation in the span-wise direction. Extrapolation of the damping-rate results delivers the value of the Reynolds number for amplification of the wake mode, as $Re_{crit,2D} \approx 905 \pm 2$, a result that has been found to be consistent with that delivered by the two-dimensional DNS. Summarizing the results of the present section (Abdessemed, Sherwin and Theofilis 2004), BiGlobal instability analysis of two-dimensional perturbations predicts the least-damped wake eigenmodes, whose function is to lead the steady two-dimensional basic state to unsteadiness through a Hopf bifurcation. As such, the natural extension of the work from this point is to enquire the predicted scenario in the context of three-dimensional ($\beta \neq 0$) BiGlobal instability. If unstable 3D eigenmodes were to exist, the Hopf scenario will be of academic value, since three-dimensional flow would become unstable before the Hopf bifurcation could be reached (c.f. the lid-driven cavity flow; Theofilis 2000). Otherwise, one possible mechanism leading flow to transition should be sought through Floquet analysis of the periodic basic state which ensues the first two-dimensional bifurcation (c.f. the cylinder flow; Barkley and Henderson 1996).

Figure 13: Disturbance vorticity of the least-damped (β=0) wake BiGlobal eigenmode of LPT flow
at $Re = 820$ (left) and $Re = 895$ (right).

Figure 14: Prediction of $Re_{crit,2D}$ by the structured- and the hybrid-mesh analyses of instability of the two-dimensional (β=0)
BiGlobal eigenmode

Reynolds number
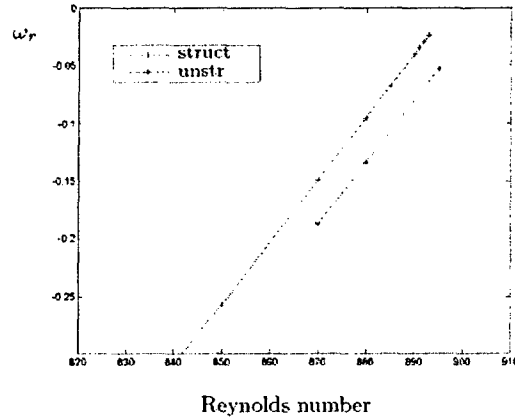
     The wake mode of the LPT flow is reminiscent of that in the wake of the circular cylinder (Morzynski, Afanasiev and Thiele 1996) and in the wake of the NACA0012 airfoil (Theofilis *et al.* 2002) and deserves some discussion of its characteristics. Assuming it were technically impossible to perform a BiGlobal instability analysis, one might have attempted to obtain the eigendisturbances of the flow in the wake of the LPT blade by applying classic Reyleigh- or Orr-Sommerfeld-based instability analysis to *slices of the basic flowfield, taken normal to the direction of the flow at different downstream locations in the wake.* We claim that, when reconstructed on a slice-by-slice basis, the resulting leading eigenmode would probably show a similar spatial structure of the amplitude functions of the disturbance quantities. In turn, the basic wake flow itself could have been modeled by appropriate (one-dimensional) basic flow models of the wake at different downstream locations, without substantial changes in the eigenmodes' structure.

However, the inflectional nature of the wake profiles in the context of classic theory would have resulted in amplification-rate characteristics that might have been different from those predicted herein. One might think that *strong instability* could result, according to either inviscid or viscous linear theory pertinent to parallel flows. Such an instability would point to spatial amplification along the downstream direction of the leading eigenmode corresponding to the locally-parallel basic flow. However, in the context of the present BiGlobal instability analysis, such "amplification" is only a partial aspect of the spatial distribution of the amplitude function of the global eigenmode, which is *stable*.

3.2. *Three-dimensional BiGlobal instability analysis of steady 2D basic flow in the LPT passage*

Three-dimensional BiGlobal instability analysis has been performed at several subcritical Reynolds numbers, in the vicinity of $Re_{crit,2D}$ using a spanwise wavenumber, β, associated with the extent of the domain in that direction, L_z by $L_z = 2\pi / \beta$. Parametric studies were performed by changing β at fixed Re. Results are shown in Figure 15, where each symbol represents a constant Reynolds number, as indicated on the plot. All real-parts of the eigenvalues remain negative, with a tendency toward the positive complex plane for increasing Reynolds number and decreasing β, suggesting that *three-dimensional linear instability does not occur below* $Re_{crit,2D}$. The eigenvalues obtained for $L_z \leq 2/3$ are real, the ones obtained for $L_z > 1$ are complex. Interestingly, it appears that the long-(spanwise)-wavelength results shown in Figure 15 are associated with the wake mode, as known from the two-dimensional analysis (c.f. Figure 13). On the other hand, the short-wavelength results shown in Figure 15 to peak around $L_z \approx 2/3$ are associated with an instability arising in the trailing-edge region, where separation of the basic state occurs. The disturbance vorticity of this eigenmode is presented in Figure 16; we term this the ***bubble*-mode** instability, since it peaks in the trailing-edge laminar separation bubble region highlighted in Fig. 10.

Figure 15: Summary of three-dimensional BiGlobal instability analysis results; plotted are the damping rate ω_r as a function of the spanwise wavenumber L_z
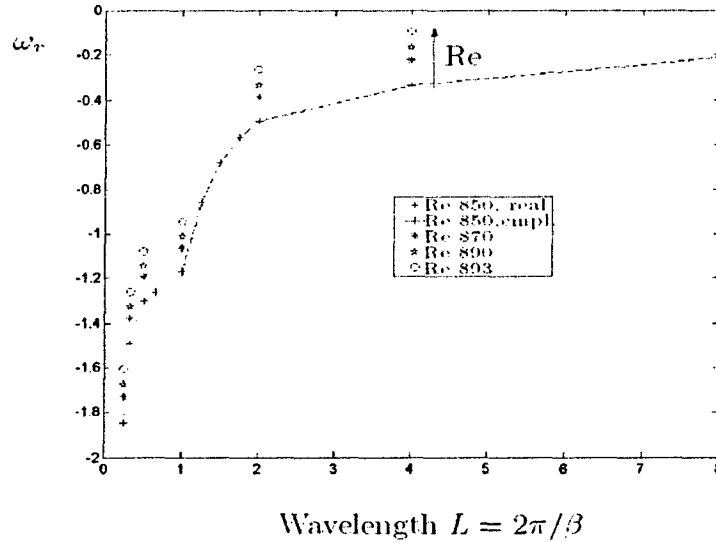
Wavelength $L = 2\pi/\beta$

Figure 16: Amplitude function of the disturbance vorticity of the least-damped three-dimensional BiGlobal eigenmode pertaining to O(1) spanwise periodicity lengths at $Re = 893$, termed the **bubble mode**, with the trailing-edge separated region highlighted.
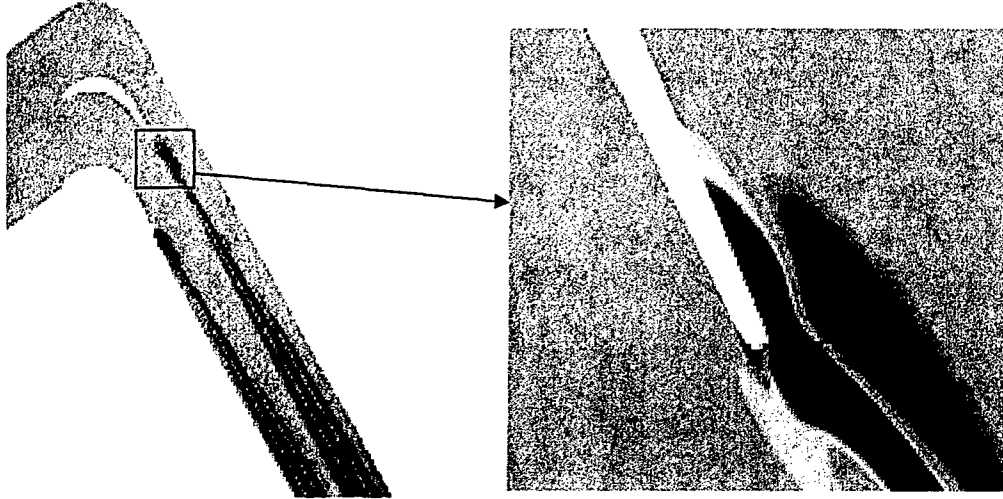
The key characteristic of the bubble mode is that *it connects disturbances in the trailing-edge separation region with that in the entire wake of the blade*. As such it provides means for connecting unsteadiness in the separation region with that in the wake, via the eigenmode frequency. Unlike the wake-mode, the three-dimensional nature of the bubble-mode could be related with vortex-shedding, via the scenario discussed by Theofilis *et al.* (2000). Indeed, the structure of the eigenmode in the separation region is reminiscent of the global eigenmode discovered by Theofilis *et al.* (2000) on the adverse-pressure gradient laminar separation bubble and that discovered by Theofilis and Sherwin (2001) on the trailing edge of the NACA-0012 wing at an angle of attack. However, interesting as this may be, the bubble-mode is stronger damped than the wake mode at Reynolds number values subcritical to $Re_{crit,2D}$ such that it can be asserted that the transition scenario on the T-106/300 LPT blade, discovered in the present work, is analogous with that of the prototype bluff body flow, namely the circular cylinder. In the LPT flow too, if there were to be a three-dimensional linear instability, it would develop as linear superposition of Floquet eigenmodes upon the time-periodic basic state set up past amplification of the first two-dimensional (wake) mode. We proceed to examine this scenario next.

4. Three-dimensional instability analysis of two-dimensional periodic basic states

4.1. *Validation of a Floquet instability analysis methodology in the circular cylinder*

A stepping stone toward the analysis of the flowfield in the LPT blade has been the well-studied case of the circular cylinder. Instability results have been reproduced on the cylinder over wide parameter ranges; an example of the Floquet multipliers obtained is shown in Table 5 at Re = 200 and distinct spanwise periodicity lengths, L_z. It may be seen that a range of $\mu > 1$ exists and peaks around $L_z = 4$, which corresponds to the well-known mode-A of the cylinder, discovered by Barkley and Henderson (1996). The basic state behind the cylinder, as well as the amplitude function of the disturbance vorticity of the leading A-mode are depicted at one instant of their periodic motion in Figure 17 (Abdessemed, Sherwin and Theofilis 2005).

26

Table 5: Floquet multipliers μ as function of spanwise periodicity length L_z in the circular cylinder at Re = 200.

L_z	3	4	5	6
μ	0.93	1.16	1.06	0.97

Figure 17: Spanwise vorticity component of mode-A of the circular cylinder at Re=200, L_z = 4.
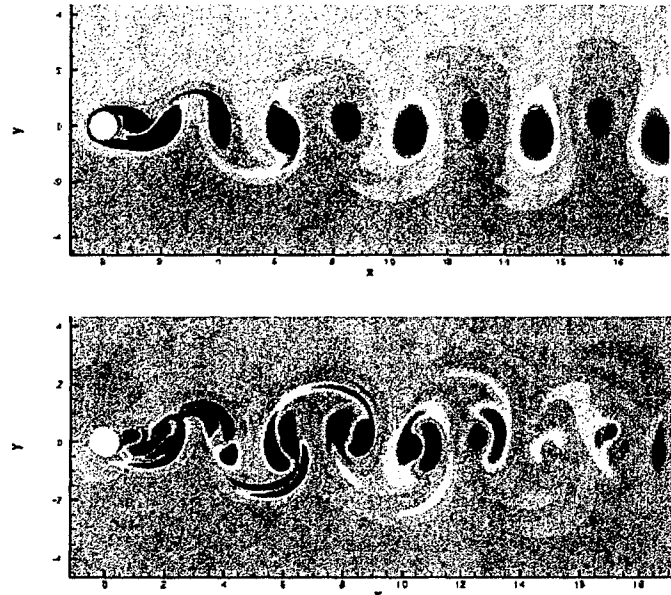
4.2 Grid-independence studies in the T-106/300 LPT blade

Preliminary Floquet instability analyses of the time-periodic basic flows in the LPT blade at $Re > Re_{crit,2D}$ have indicated instability at a specific range of parameters around Re = 2000, L_z = 8. The Floquet multipliers obtained were confirmed to correspond to unstable three-dimensional perturbations, $\mu > 1$, under a variety of h- and p-refinements. In addition, the study of effect on the eigenvalues (the Floquet multipliers) of different domain sizes was repeated in the context of the present secondary BiGlobal instability analyses; the results are shown in Table 6. Here too, it is seen that the baseline hybrid mesh is adequate for the efficient description of secondary instability and has, thus, been used throughout the subsequent analyses.

Table 6: Dependence of the leading Floquet multiplier on the mesh extent at Re = 2000, L_z = 8.

Mesh Extension	Floquet multiplier μ	Mesh Extension	Floquet multiplier μ
Baseline – "0"	1.00135	Baseline – "0"	1.00135
Inflow "1"	1.00100	Outflow "1"	1.00187
Inflow "2"	1.00142	Outflow "2"	1.00163

4.3 *Discretization of the time-periodic orbit*

As mentioned in Section III, the Floquet secondary analysis introduces one additional parameter into the stability problem, namely the period of the basic state, over which secondary instabilities develop. This period must be captured adequately by resolving a large number of snapshots of the flow within one period and monitoring the results of the resulting coupled secondary eigenvalue problem by Floquet theory. However, the larger the number of these snapshots, the larger the size of the coupled eigenvalue problem becomes, such that efficiency considerations suggest the use of an optimum discretization of the periodic orbit. In order to identify this optimum, while ensuring that the time-dependent state is captured adequately over one period, analyses have been performed in which the periodic orbit was discretized using 8, 16 or 32 snapshots. Typical results at Re=2000, L_z = 0.3 are shown in Table 7 where it can be seen that four significant figures of μ are recovered in all computations. In the following analyses 16 time-slices have been used, implying convergence of the Floquet multiplier in 7 significant places.

Table 7: Sensitivity of the leading Floquet multiplier on the discretization of the periodic orbit at $Re = 2000$, $L_z = 0.3$.

Time slices	8	16	32
μ	0.883832	0.883892	0.883892

4.4 *Analysis of a periodic row of pairs of T-106/300 LPT blades*

A different angle of the problem of instability of the object at hand is considered next, namely partial relaxation of the conditions of periodicity, used up to and past the present point. The results should serve as a warning on the sensitivity of stability calculations on boundary conditions, at least within the EVP framework; they certainly set the stage for the results presented in Section IV. 6.

The situation is illustrated in Figure 18, where two baseline domains have been placed together and resolved as a single basic flow under the boundary condition of periodicity as indicated. The basic flow obtained at Re = 2000 is also shown in Fig. 18. This numerical experiment was put forward since the periodicity in the wake introduces the possibility of phase-shifts between the two wakes, an issue that is clearly absent in the analysis of steady basic flows. In turn, the resonance potential that is introduced on account of these phase shifts may give rise to subharmonic behavior absent from the single-blade configuration. Indeed, it can be seen in Fig. 18 that there are no major interactions between the two wakes; however, an important observation is a slight phase lag between the shedding of the flow past the upper and the lower blade, which shows that indeed subharmonic effects occur in rotationally symmetric turbine flows.

Next, the question of potential influence of this effect on the leading Floquet multipliers is addressed; the results are presented in Table 8. Both results presented have been confirmed to remain unchanged under p-refinement. Comparing the results obtained on the baseline with those on the extended domain reveals one important qualitative difference: *the absence of interaction of the periodic wakes yields unstable eigenvalues; relaxing this constraint leads to flow that remains linearly stable* - for all Reynolds numbers examined. Hence, linear instability may be dependent on the periodic boundary conditions, generally assumed to be valid in turbine flows. Accepting the limitations of the model, the baseline domain has been considered in the subsequent analyses.

Figure 18: Grid and basic flow solution around a two-blade periodic system at Re=2000.
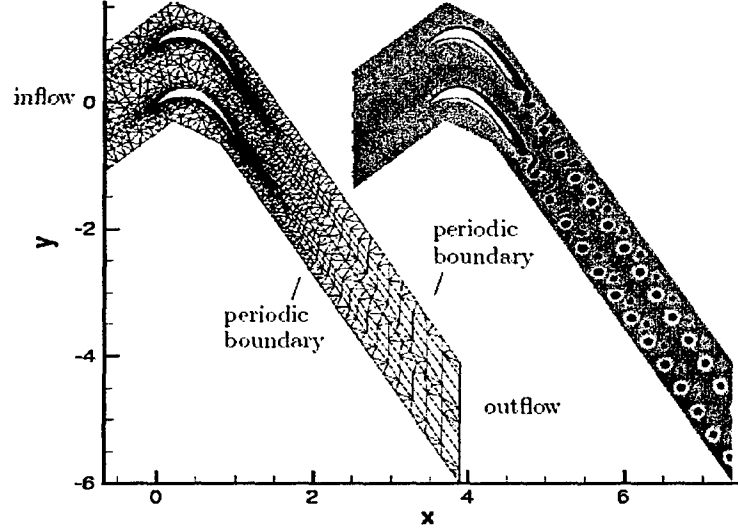
Table 8: Dependence of the leading Floquet multiplier on the mesh extent at $Re = 2000$

L_z	μ Single blade	μ Two blades
0.3	0.8839	0.8822
0.4	0.8775	0.8755
4	1.0021	0.9955
8	1.0036	0.9965
16	1.0034	0.9982
∞	0.9997	0.9993

4.5 Analysis of a periodic row of T-106/300 LPT blades

In the following, Floquet multipliers μ have been computed for different periodicity lengths L_z of three-dimensional disturbances at several Reynolds numbers $Re > Re_{crit,2D}$, i.e. above the Hopf bifurcation. Figure 19 summarises the results for the first two eigenmodes of a parametric study at two Reynolds number values, one right after the two-dimensional transition, $Re = 920$, and one at a higher Re-value, $Re = 2000$, for comparison. We recall that Floquet multipliers below 1 indicate a decaying (periodic, three-dimensional) perturbation whereas $\mu > 1$ are associated with an unstable solution. By contrast to the analysis of a steady basic flow, all leading Floquet multipliers μ remain real, indicating *time-locking of three-dimensional perturbations* which develop upon the time-periodic basic state with the frequency of that basic state. The respective most unstable spanwise periodicity length, $L_{z,max}$ is indicated on the lower-Re plot, having been defined by the condition $\partial \mu / \partial L_z \approx 0$. In addition, the critical condition $L_{z,crit}$, defined by the location at which the Floquet multiplier exceeds $\mu = 1$, is also indicated. In both the low and the higher Reynolds number values, the periodic flow becomes unstable to three-dimensional perturbations at about the same value of $L_{z,crit} \approx 4$.

Significantly, the first three-dimensional instability occurs immediately after two-dimensional transition. This instability is characterised by long-wavelength perturbations as can be seen in the results at both Reynolds numbers. An indication of the accuracy of the Floquet analysis performed herein is obtained in the limit $L_z \to \infty$ ($\beta \to 0$) at the present two and all other Reynolds numbers examined but not presented in this figure. As can be seen in the results of Fig. 19, in this limit the growth-rate approaches $\mu = 1$, which represents the fact that the three-dimensional perturbation field vanishes in this limit and the total field returns to the periodic two-dimensional basic flow.

Figure 19: Dependence of Floquet multipliers on the spanwise periodicity length at Re=920 (left) and 2000 (right).
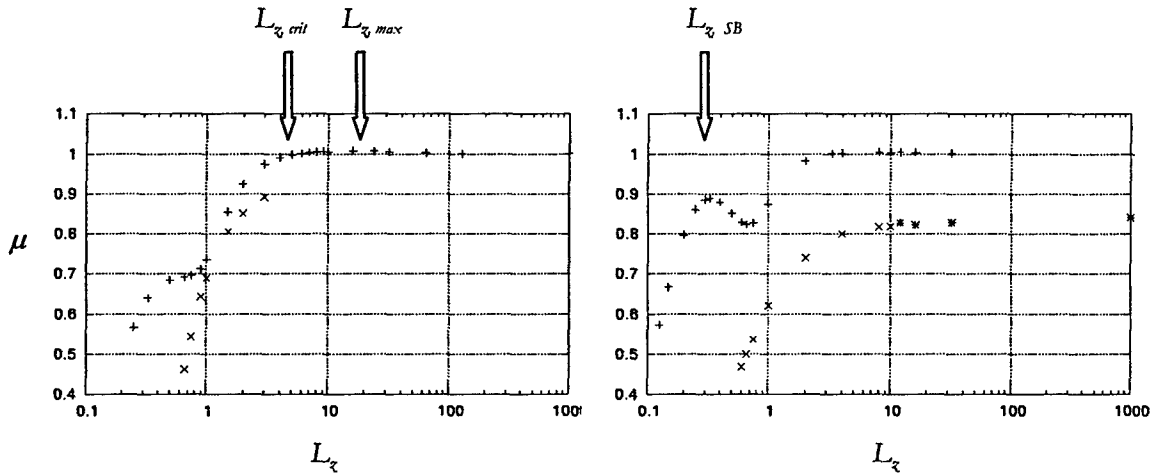
Finally, in both sets of results the short-periodicity-length (large-wavenumber) perturbations corresponding to $L_z < 1$ appear to belong to a mode distinct from that which becomes unstable at $L_z \approx 4$. The monotonic dependence of the leading Floquet multiplier on the spanwise wavenumber at low Reynolds numbers changes in character and a second local maximum at $L_z < 1$ is found, which evolves such that an inflection point in the dependence of μ on L_z appears as the Reynolds number increases. This maximum is associated with short wave lengths while the eigenfunction remains stable for all Reynolds numbers considered. However, the amplitude functions are a weak function of the Reynolds number; Figure 20 shows the basic flow and the disturbance vorticity, as two instances during the period, at $L_z = 0.3$ and Re = 2000. Strong analogies may be seen between these results and mode-A of the flow past a cylinder, shown in Figure 17. In both cases the local maxima of the amplitude functions are concentrated in the spanwise vortex cores of the respective basic states. Seen from the perspective of classic linear theories, well-known instabilities such as the vortex core and shear-layer instabilities may be identified as partial features of the BiGlobal eigenmode discovered here. Furthermore, in comparison with the cylinder flow, a spatio-temporal symmetry can be established by comparing the eigenmode with itself after half an oscillation period, $q(x, y, z, t) \approx q(x, y, z + Lz/2, t + T/2)$. However, by contrast to the flow past a cylinder, the instability discovered in the LPT blade is characterised by relatively small growth rates, and the maximum Floquet multipliers obtained do not grow significantly with increasing Reynolds number. Finally, in view of the relatively high concentration of disturbance energy in the trailing edge separation region, this mode is a prime candidate for transient growth analyses, presented in Section IV. 6.

30

Figure 20: *Left:* vorticity of the periodic basic flow at Re=2000. *Right:* disturbance vorticity of the least-damped Floquet eigenmode at L_z=0.3; snapshots taken half a period apart from each other.
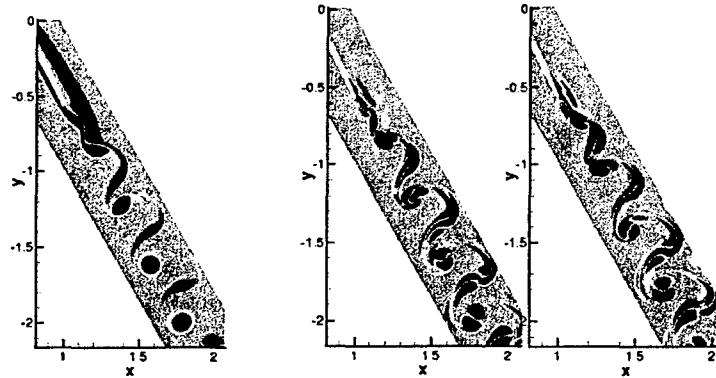
A qualitative overview of the flowfield resulting from amplification of the most unstable Floquet eigenmodes is shown in Figure 21, in terms of the (spanwise) basic flow vorticity and that of the disturbance field at two combinations of Reynolds number and spanwise periodicity wavelength. The characteristic vortex pairs in the basic state are clearly visible, as is the structure of eigenmodes corresponding to such a basic field.

Figure 21: Vorticity of the basic state (upper) and the perturbation field (lower) at two parameter combinations resulting in instability, (Re=910, L_z=16 – left) and (Re=2000, L_z=12 – right).
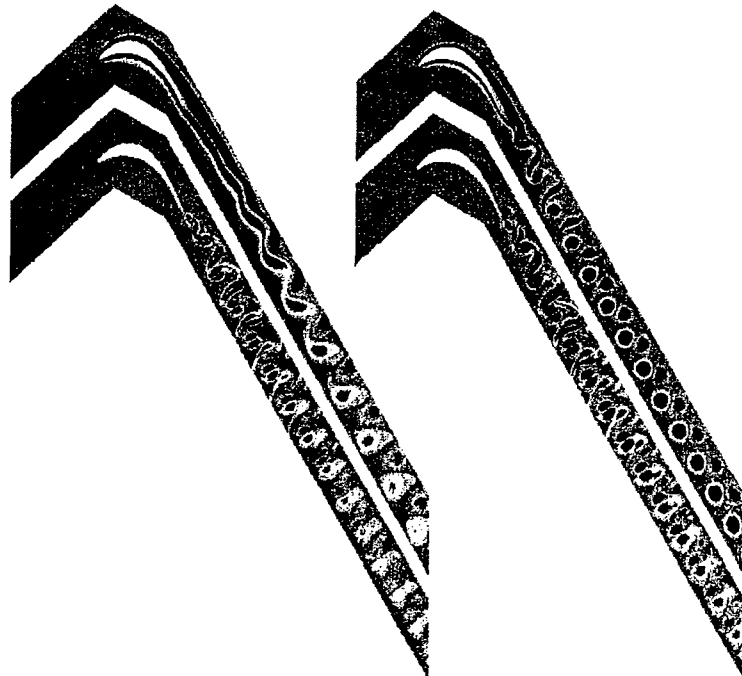
By contrast, in Fig. 20 one may see that the wake is composed of pairs of isolated vortices connected by shear layers. As such, connections may be attempted with results of classic one-dimensional linear theory, which can deal with all three instability phenomena, the elliptic instability of vortex pairs, instability of isolated vortices and that of shear layers. Such a connection may be possible, especially in the far-wakes of the flows shown in both figures 20 and 21, but will not be attempted here. Instead, the point of view is taken that such instabilities are *parts of a single eigenmode*, namely that presently resolved by secondary BiGlobal analysis. This argument is supported by the fact that the near-wake field has a rather complex structure, which can only be resolved by the large-scale computations performed in the framework of BiGlobal analysis, or DNS. If conclusions on the instability properties in the wake are sought, especially in terms of frequencies to be utilized for flow control, the structure of the entire wake must be taken into account, otherwise erroneous results could be obtained. A similar conclusion has been reached in the instability analysis of a much simpler vortex pair by Hein and Theofilis (2004).

Next, it is of interest to identify the neutral curve for secondary instability of the time-periodic flow. This result is shown in Figure 22 in terms of the dependence of the critical spanwise wavelength on Reynolds number. The overall minimum value for three-dimensional instability of the time-periodic flow occurs at the critical conditions ($Re = 1400$, $L_{z\,crit} = 2.4$). The shape of the curve obtained is plausible for low Reynolds numbers, at which the flow has been found (in Section IV.3.2.) to be stable with respect to BiGlobal instability below $Re_{crit,2D}$. One may also accept the prediction that the flow is stable for very low spanwise periodicity lengths; however, it is intriguing indeed, that high Reynolds number results are becoming stable with respect to both small- and medium-wavelength three-dimensional perturbations. Owing to the cost of the computations presented here, this result has not been investigated further.

Figure 22: Neutral curve for amplification of three-dimensional secondary instabilities in the T-106/300 LPT blade.
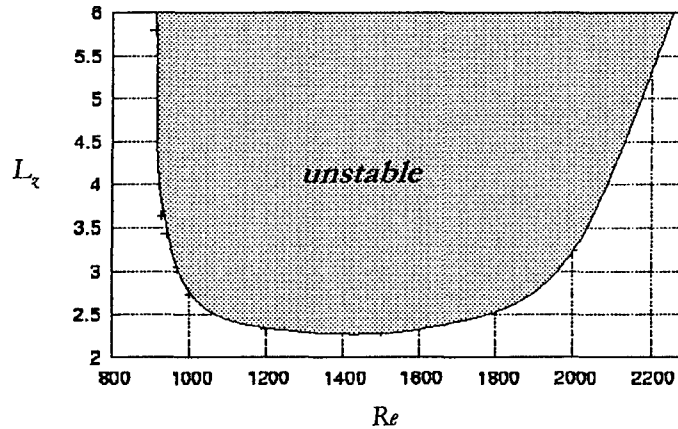
The spatial structure of the amplitude functions of the spanwise disturbance vorticity pertinent to the leading Floquet eigenmodes is shown in Figures 23 and 24, respectively for two Reynolds numbers values, 1000 and 2000. In all results the predominance of disturbance activity in the wake is clearly seen although, as mentioned, it is only the short-wavelength mode associated with the trailing-edge separation for which *the origin of such activity can be traced in the trailing-edge separation region.*

Figure 23: Amplitude function of the disturbance vorticity of the leading Floquet eigenmodes at Re = 1000.

Unstable Long-Wavelength "Stationary" 1st Mode

Stable Short-Wavelength "Stationary" 1st Mode

Stable Traveling 2nd Mode
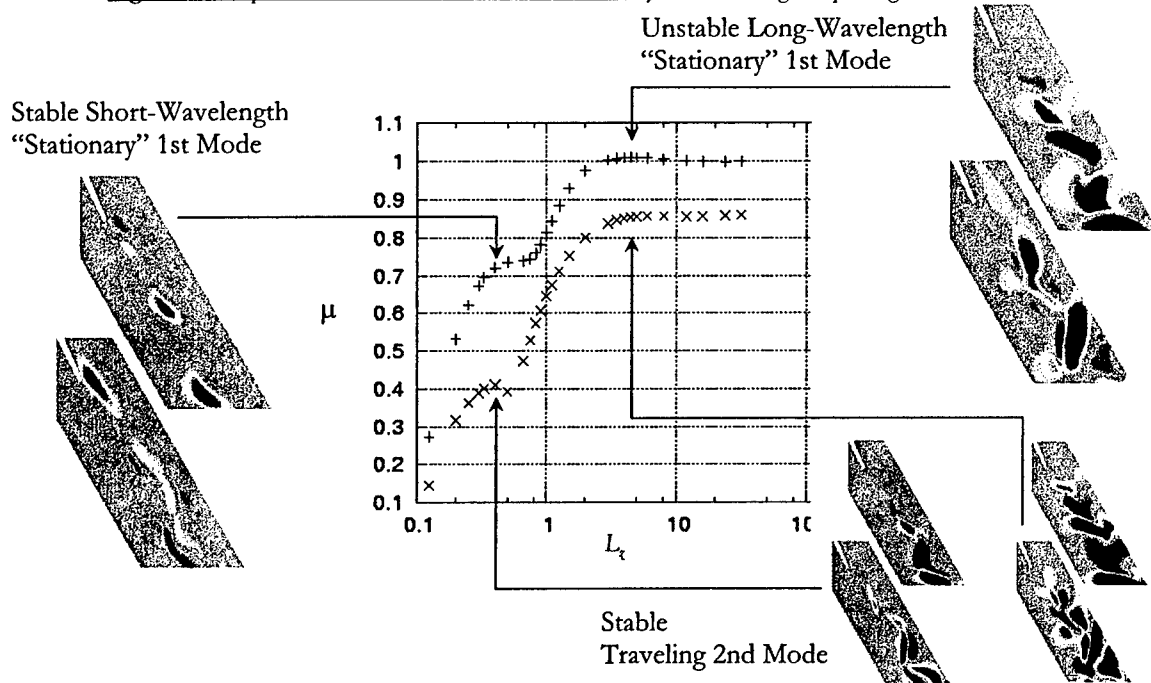
Figure 24: Amplitude function of the disturbance vorticity of the leading Floquet eigenmode at Re = 2000.
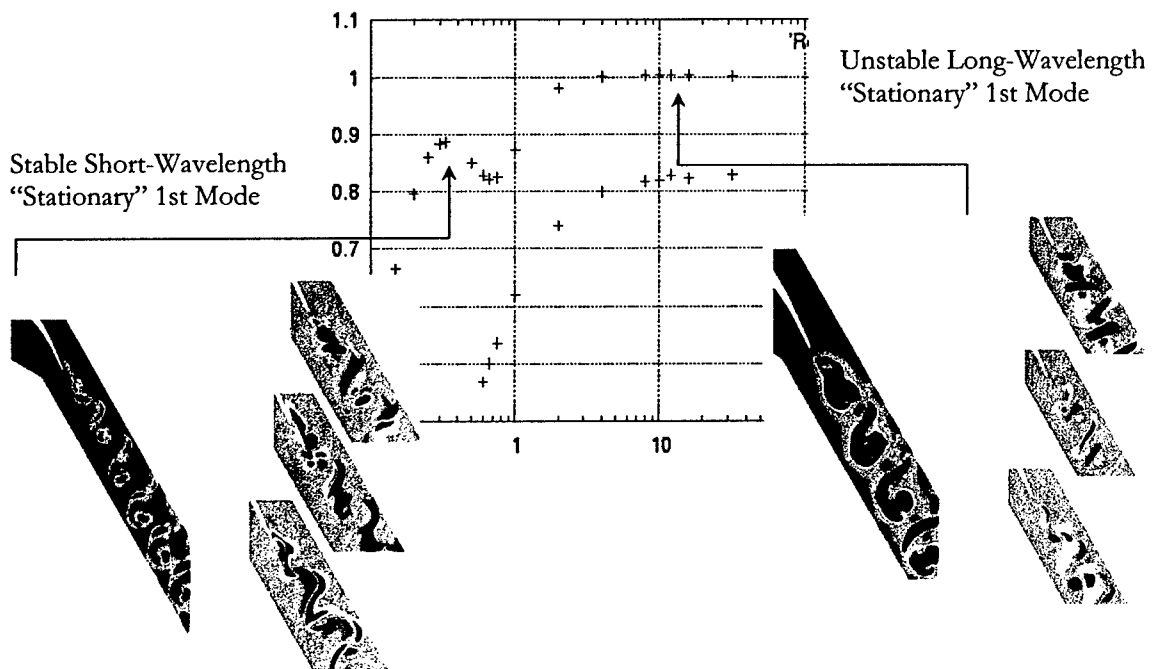
Unstable Long-Wavelength "Stationary" 1st Mode

Stable Short-Wavelength "Stationary" 1st Mode

In these and other results not presented here, it appears that the trailing-edge separation region is actively involved in two processes, the generation of secondary instability and the connection of such instability on the surface of the blade with that in the entire wake. Figure 25, in which the amplitude function of the disturbance vorticity is shown, clearly demonstrates this fact at a single Reynolds number value $Re = 2000$; in both eigenmodes the connection of the disturbance flowfield in the trailing-edge separation region with that in the wake is clearly visible. This connection should prevent further attempts by classic theory to treat the two aspects of the same BiGlobal eigenmode, namely global instability in the trailing-edge separation region and quasi-local instability in the wake, as distinct instability mechanisms that occur in different parts of the flow. The question whether instability at the trailing edge gives rise to that in the wake or vice versa is, in the author's view, ill-posed; the present results indicate that the elliptic partial-differential-equation-based secondary BiGlobal eigenvalue problem admits solutions that simultaneously affect both regions in the flow; attempts to isolate and treat independently the different flow instability mechanisms would lead to incomplete and erroneous results.

Figure 25: Least-stable, short-wavelength (left) and most unstable long-wavelength (right) eigenmodes at $Re = 2000$.

Summarizing, the trailing-edge separation region has been found to be active in flow instability of both the primary steady and the secondary time-periodic flow. The lack of linear amplification within an eigenvalue problem solution is by no means diminishing the value of this discover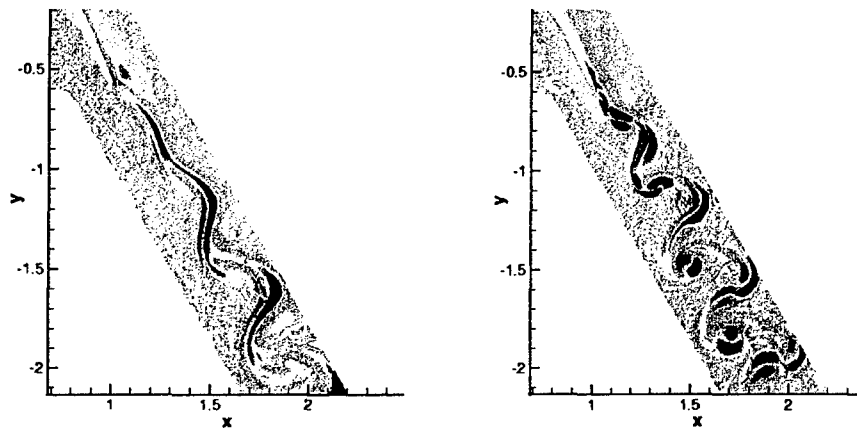y. Indeed, in subsequent transient growth analyses, for which information on the full eigenspectrum – and in particular on damped eigenmodes – is necessary, the present identification of the distinct members of the eigenspectrum has been demonstrated to be of central importance, as will be shortly discussed in Section IV. 6. Further, the present results on the potential of laminar separation to generate global instability complete the picture originally put forward by the work of Theofilis (1999) and Theofilis et al. (2000) on the global instability of a laminar separation bubble developing on the flat plate under adverse pressure gradient, a scenario that was later discovered to be operative on the NACA 0012 airfoil at an angle of attack (Theofilis *et al* 2002). Here, the same phenomenon is found to occur in the trailing-edge separation region of the LPT flow, as BiGlobal eigendisturbances of both the steady- and the time-periodic basic flows, as schematically summarized in Figure 26. The present result extends and further strengthens the discussion of Theofilis, Sherwin and Abdessemed (2004) regarding the unifying perspective of global instability of laminar separation bubbles in the three applications; the novel element here is the applicability of the arguments presented on the basis of analyzing steady laminar separation to instability of time-periodic separation bubble flows as well.

Figure 26: Amplitude function of the spanwise (3D) disturbance velocity component of the global eigenmode of 2D separation bubble flow: (a) adverse-pressure gradient flat plate flow, (b): steady flow in the trailing-edge of a NACA 0012 airfoil at an angle of attack, (c): steady flow on the trailing-edge of a T-106/300 LPT blade, (d): time-periodic flow on the trailing-edge of a T-106/300 LPT blade.
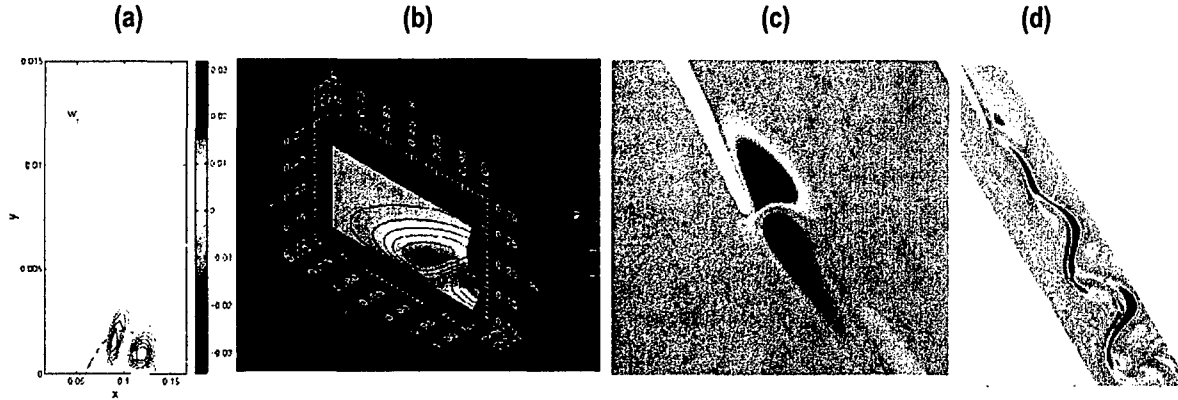
Finally, in view of the significance attached to the potential of the separation bubble on the trailing-edge of the LPT blade to sustain global instabilities, Figure 27 presents the dependence of the wavelength at which short-wavelength secondary BiGlobal instability originating at the trailing-edge separation region reaches its maximum, $L_{z\,max,\,SB}$, on Reynolds number. Interestingly, while at the lower Reynolds number values there is a decrease of $L_{z\,max,\,SB}$ with increasing Re, at the highest Reynolds number values examined, of $O(5000)$, this quantity appears to reach a plateau at a low level, $1/4 < L_{z\,max,\,SB} < 1/3$. Since, the larger the Reynolds number the more relevant the present results become to actual applications, it is worth mentioning here that a spanwise periodicity length of less than a chord length may be realizable in practical situations.

Figure 27: The dependence of $L_{z\,max,\,SB}$ on Reynolds number.
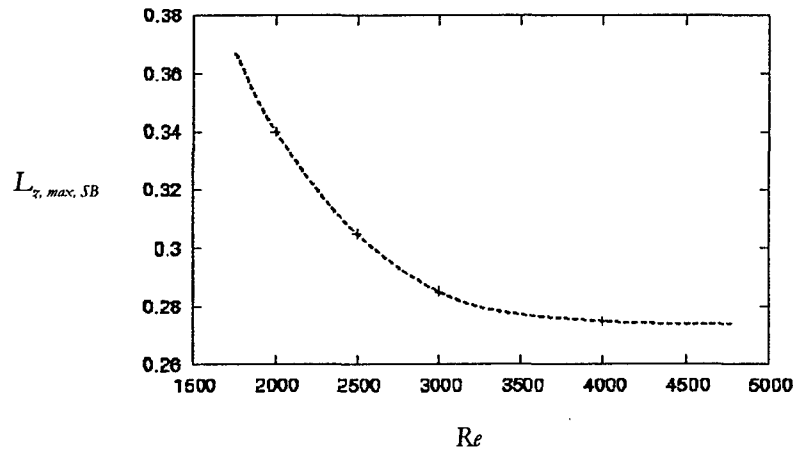
Indeed, the key assumption of the present analysis, namely homogeneity of space in the spanwise direction, which in the framework of BiGlobal instability permits consideration of a Fourier decomposition along z, can only be relevant to the actual three-dimensional blade geometry, *if the spanwise direction permits accommodation of small wavelengths that are small enough for several periods to fit within*; in the present results such wavelengths have been identified, which raises an issue that is worth examining experimentally.

A final aspect related with global instability of the separation region is highlighted next. Superposition of the least-damped mode upon the time-periodic basic state in the neighborhood of the trailing-edge of the blade at Re=2000 is shown in Figure 28. In the same figure isosurfaces of vorticity magnitude indicate three-dimensionalization of the flowfield downstream of the trailing edge, alongside vortex-shedding in the wake of the LPT blade. The latter mechanism has been one of the hallmarks of global instability in the primary reattachment zone of the separation bubble on the flat plate (Theofilis *et al.* 2000) and has also been found to be operative in the present T-106/300 LPT flow.

Figure 28: *Left:* Snapshot of the least-damped Floquet eigenmode superimposed upon the time-periodic basic state at Re=2000. *Right:* Three-dimensionalization and concurrent vortex-shedding in the wake of the LPT blade.
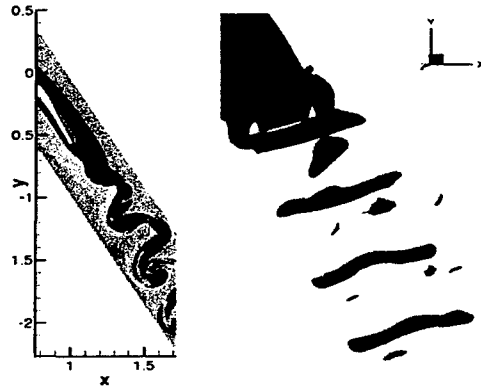
5. Three-dimensional DNS of two-dimensional periodic basic states

The consistency of the results obtained by Floquet-analysis with those delivered by three-dimensional DNS has been established. Validations on the cylinder were first performed (but not shown here) in which the Floquet analysis results of Barkley and Henderson (1996) were reproduced by the present three-dimensional DNS. Subsequently, attention was focused on the LPT flow, at a single Re=2000. An initial condition for the DNS has been constructed, composed of a two-dimensional Floquet-mode at several spanwise periodicity lengths, which has been superposed upon the basic state at a low amplitude, A=10^{-5}. For consistency with the Floquet approach, the solution in the spanwise direction has been approximated by the first non-constant Fourier-mode.

Table 9: Comparison of amplification rates (Floquet multipliers) obtained from Floquet analysis (μ) and 3-d DNS (μ_{DNS}).

L_z	0.2	0.3	0.75	4
μ	0.795	0.8839	0.8247	1.0004
μ_{DNS}	0.797	0.8846	0.8261	1.001

One comparison of the Floquet multiplier μ obtained from Floquet analysis and the equivalent measure obtained from the three-dimensional DNS, μ_{DNS}, is shown in Table 9, where a satisfactory agreement of these quantities may be observed. Figure 29 illustrates the decay of the disturbance energy with time for different wavelengths L_z, with the underlying period of the basic state clearly visible. The energy of the field corresponding to $L_z = 4$, predicted by the Floquet analysis to be unstable, may be seen to increase with time in this figure, while that of the other three modes clearly corresponds to decaying perturbations. This cross-validation of our DNS and Floquet analysis tools will become useful in the subsequent transient growth analysis, in a manner that will be discussed in the next section.

Figure 29: Time evolution of the DNS signal for the four wavelengths shown in Table 9.
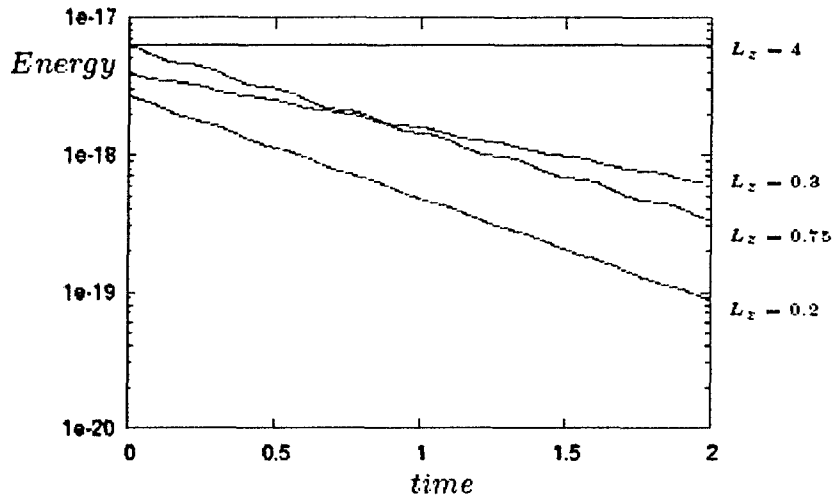
6. Transient Growth analysis

In what follows, the first-ever transient growth (TG) analysis results of a nonparallel flow are reported. While the theory pertinent to one-dimensional ("parallel flow") profiles is well-developed (Schmid and Henningson 2001), to-date no transient growth analysis of essentially nonparallel flows ("BiGlobal TG") has been reported in the literature; *the present work is the first such effort.* BiGlobal TG analysis proceeds by computing the pseudospectrum of the matrix discretizing the linearized disturbance equations, A, via computation of the eigenspectrum $\{z\}$ of this matrix A, perturbed by a small amount, according to

$$(A+E) \; x = z \; x.$$

Here E is of the same dimension as A and contains elements of order ε. Schmid and Henningson (2001) use the definition of the norm $\|E\|$ in order to quantify the perturbation of A, which may be related with the present simpler definition.

In the following, results are presented of linear stability analysis of the perturbed system, using the tools exposed in the previous sections. Here, steady flow at a subcritical Reynolds number $Re = 820$ is considered, requiring only solution of the BiGlobal eigenvalue problem. Ideally, the full spectrum of the perturbed matrix should be computed within a TG analysis, in order to assess the potential of different parts of the eigenspectrum to sustain the TG phenomenon. Note that in the case of wall-bounded shear flows, it is the strongly stable members of the eigenspectrum in the intersection of the eigenvalue branches that exhibit the highest sensitivity.

In the nonparallel basic flow problem at hand, the computing cost of the Arnoldi approach used scales with the dimension of the Krylov subspace utilized, such that computation of a large number of eigenvalues is impractical. On the other hand, if TG manifests itself in the resolved part of the eigenspectrum, one can safely assert that perturbations of the matrix of at least the order of magnitude used to unravel TG in the resolved- would lead to TG in the full-spectrum as well. Consequently, the spectrum of the first few eigenvalues (typically of O(10)) has been obtained at a spanwise periodicity length $L_z = 1/3$ and $\varepsilon = 0$.

Figure 30: The BiGlobal eigenspectrum of LPT flow at Re = 820, $L_z = 1/3$.
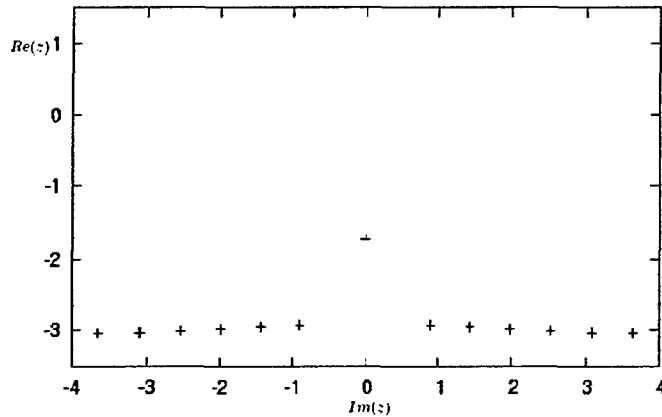
All eigenmodes, shown in Figure 30, are strongly stable, as discussed in Sections IV. 3.1 and 3.2. The least-damped (stationary) mode has been identified to correspond to the "bubble" mode, while the next in significance, from a stability analysis point of view (traveling) mode is the "wake" mode previously discussed. The damping rate of the bubble mode is of $O(-2)$, meaning that if such a perturbation were to be introduced into the flow at a small, linear amplitude, say $A_0 = O(10^{-4})$, it would take a time $\Delta T = O(-\ln(10^{-12})/2) \approx 14$ (units scaled with the free-stream velocit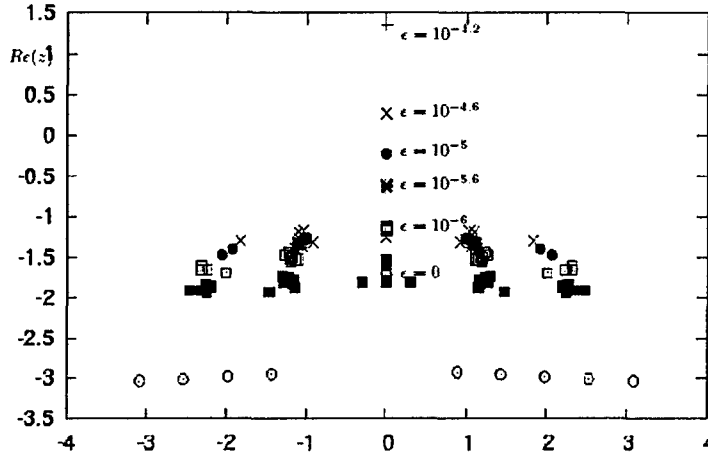y and the chord length) for the perturbation to subside to machine accuracy levels $A_f = O(10^{-16})$; if introduced at $A_0 = O(10^{-6})$, the time elapsing for the perturbation to reach machine zero would be $\Delta T = O(-\ln(10^{-10})/2) \approx 11.5$.

Figure 31: The BiGlobal pseudospectrum of LPT flow at Re = 820, L_z = 1/3, obtained by a small number of exploratory computations.

However, a very different picture emerges from the pseudospectrum analysis. Figure 31 shows the leading five pseudo-eigenvalues for different perturbations of order $\varepsilon \in [10^{-6}, 10^{-4}]$, units scaled with the free-stream velocity. While the traveling disturbances are mildly affected by matrix perturbations in this range, **the pseudo-eigenvalue corresponding to the bubble mode has a zero-crossing.** In other words, perturbations of $O(10^{-4})$ in the original matrix suffice to result in linearly unstable flow through a BiGlobal TG mechanism, although linear BiGlobal theory based on the EVP predicts strong stability. A systematic set of computations of the same phenomenon, scanning the parameter range shown, results in the ability to plot the boundary curve corresponding to each level of perturbation; this is shown in Figure 32. While perturbations of $O(10^{-6})$ result in a more-or-less uniform shift of the eigenspectrum toward the $Im(z) = 0$ axis, mild subsequent increases of ε result in a strong destabilization of the bubble mode. Figure 33 shows the monotonic increase of the leading pseudo-einvalue with increasing perturbation order. These results may be used in order to interpolate an approximate matrix perturbation value for which the original linear system becomes unstable, $\varepsilon \approx 10^{-4.7}$.

Figure 32: The BiGlobal pseudospectrum of LPT flow at Re = 820, $L_z = 1/3$.
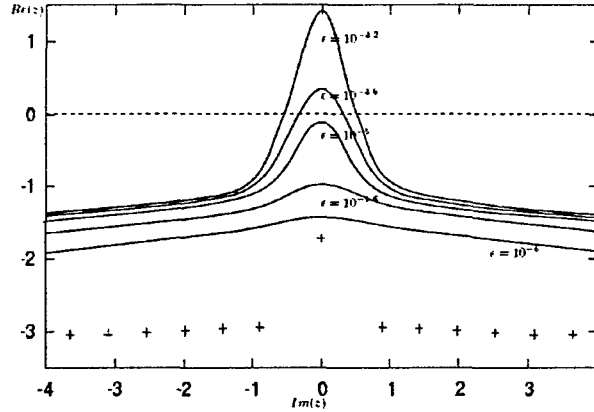
Figure 33: Dependence of the pseudo-amplification rate on the order of perturbation introduced into the matrix. Zero-crossing occurs at $\varepsilon \approx 10^{-4.7}$
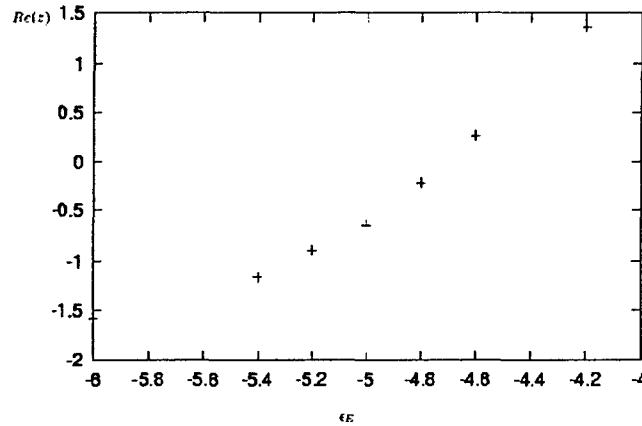
Next, it is interesting to visualize the eigenfunctions corresponding to the unstable pseudo-eigenmode. Disturbance velocities shown in Figure 34 have been scaled with the absolute maximum of the largest component, which turns out to be the transverse velocity component $\hat{v}$. Interestingly, the entire wake is involved in this instability mechanism, although, in addition, one may identify that, respectively, the trailing-edge part of the suction side of the blade in the $\hat{u}$ - and that at the pressure side in the $\hat{w}$-disturbance velocity component are also active. On the basis of these results, the disturbance energy is computed and plotted in Figure 35. Finally, initializing a three-dimensional DNS with the most unstable bubble pseudo-mode, at an amplitude consistent with that discovered by the pseudospectrum analysis, results in the characteristic of TG curve shown in Figure 36; an initial algebraic growth of the perturbation energy is followed by exponential decay. This is the hallmark of TG (albeit in a BiGlobal context here), in turn confirming the results presented on the basis of pseudospectrum analysis.

Figure 34: Upper-to-lower: velocity components $(\hat{u}, \hat{v}, \hat{w})^T$ of the amplified eigenmode of the perturbed system.

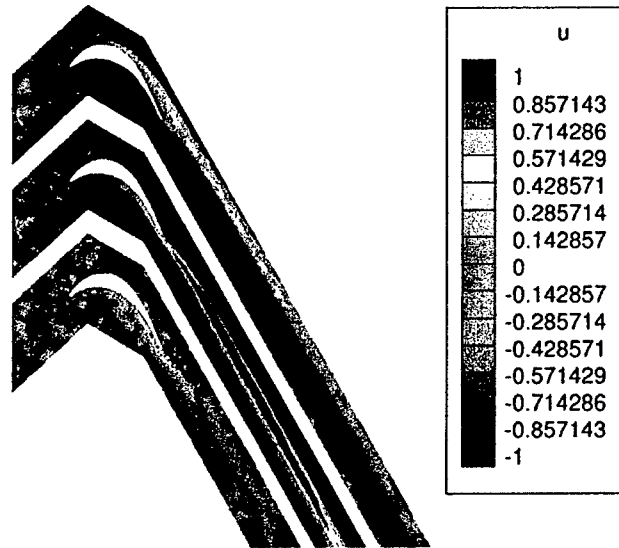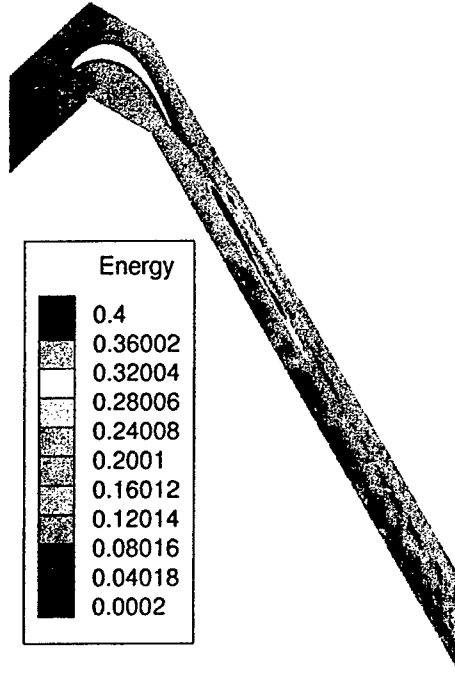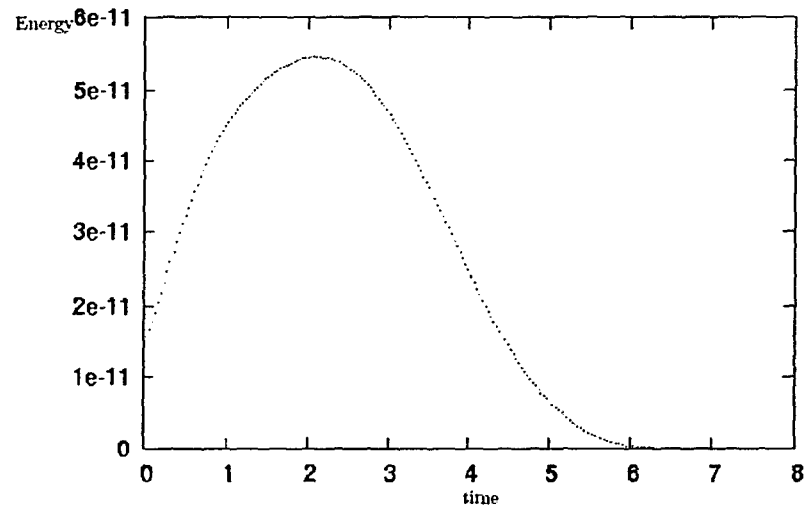**Figure 35**: Disturbance energy corresponding to the results of Fig. 34

Figure 36: Energy-growth of the most unstable perturbation at Re $= 820$, $L_z = 1/3$, Re$=820$, $\varepsilon = 10^{-4}$.

V. SUMMARY AND FUTURE DIRECTIONS

The maturing of numerical methods for the accurate description of flows in complex geometries in incompressible flow (Karniadakis and Sherwin 2005), as well as those for the solution of large eigenvalue problems in both flow regimes (Theofilis 2003) has permitted performing the first three-dimensional BiGlobal instability analyses of a low pressure turbine flow in incompressible flow. The related eigenvalue- and initial-value-problems (EVP/IVP) have been solved, the first in the context of analysis of both steady and time-periodic flows. A model T-106/300 LPT blade has been considered, in spectral/hp element tessellations of the entire domain at transitional Reynolds numbers. Inflow/outflow and periodic boundary conditions have been imposed as appropriate.

Two- and three-dimensional BiGlobal EVP-based instability analyses of steady two-dimensional incompressible basic flows over a row of T-106/300 Low Pressure Turbine (LPT) blades has been performed at chord Reynolds numbers below 900, where such basic flows exist. Both structured and unstructured meshes have been used in the context of structured- and hybrid-mesh spectral/hp element numerical methods at different degrees of grid refinement, while variations of the polynomial order with either mesh type have ensured numerical convergence. The analysis shows that the transition from steady to periodic flow takes place at a Reynolds number of $Re_c = 905 \pm 2$, as a result of a Hopf bifurcation of the least-damped two-dimensional BiGlobal eigenmode. The flow remains linearly stable to three-dimensional disturbances below Re_c. The two most interesting BiGlobal eigenmodes have been found to be related with the wake of the blade ("wake"-mode instability) and the separated flow in the trailing-edge region on the suction side of the blade ("bubble"-mode instability).

Next, using the unstructured-mesh spectral/hp element technology alone, BiGlobal secondary EVP-based analysis of the time-periodic states established past Re_c has been performed, based on Floquet theory. In addition, three-dimensional direct numerical simulations have been performed in order to independently verify the stability analysis results and follow amplified modes into transition. In both cases variation of the polynomial order of the numerical methods has ensured numerical convergence. Three-dimensional stability analyses of two-dimensional periodic states have been performed at chord Reynolds numbers $Re \in [900, 5000]$, where the leading Floquet eigenvalues have been obtained in a wide range of spanwise wavenumber parameters β. In the entire range investigated unstable three-dimensional modes have been discovered. As the 3D flow approaches the two-dimensional limit ($\beta \rightarrow 0$), the time-periodic basic state is recovered. At $\beta = O(1)$, the most significant Floquet eigenmode is qualitatively analogous with mode-A of cylinder flow (also solved herein).

Returning to low Reynolds numbers, where steady states exist, IVP-based analyses have delivered indications of strong three-dimensional transient growth. The "bubble" eigenmode identified in the EVP-based work to connect instability mechanisms in the trailing-edge separation region on the blade, has been shown to sustain strong energy growth. This result has also been independently confirmed by 3D DNS and requires further systematic research, as it points to a transition scenario that has, up to now, been neglected in stability investigations of the flow at hand. Nevertheless, its in-depth analysis can contribute to the same objective of the present research, identification of the predominant, instability-related frequencies to be used for flow control; while the EVP-based analysis has identified such discrete frequencies, the IVP-based analysis may also deliver bands of frequencies that are responsible for flow transition.

Regarding relevance of the present research to Air Force needs, it should be mentioned that in all three classes of research performed herein (EVP- and IVP-based instability analysis of steady basic flows and EVP-based analysis of time-periodic basic states) the mechanisms discovered have spanwise wavelengths that are fractions of the blade chord length. As such, the phenomena described herein may be relevant to real three-dimensional blades, in which the presently used assumption of spanwise flow homogeneity is only tenable in conjunction with amplified short-wavelength eigenmodes; it is interesting to examine this proposition by an accompanying experiment focusing on the instability mechanisms discovered in the framework of the present Grant. Regarding future extensions of the present work, besides further exploration of the IVP-based approach in incompressible flow, in the authors' view it is worth performing BiGlobal analyses in the spirit of those presented herein, also in compressible flow. Numerical methods for the description of BiGlobal instability phenomena in complex geometries are much less developed than the (incompressible) spectral/hp element method, which identifies the first challenge that needs to be tackled. Two further avenues worthy of exploration in future research are the BiGlobal instability analysis of time-averaged and turbulent flowfields. No work is known to the authors to deal with the first problem; however, the tools presented herein are directly applicable to such an extension. Regarding analysis of turbulent flows, recent work by Crouch (2005) has demonstrated the ability of BiGlobal theory to solve the problem of buffeting on a NACA-0012 airfoil at an angle of attack and transonic Mach numbers. The payoff of a successful extension of numerical methods for BiGlobal analyses to deal with compressible flows over complex geometries and, possibly, turbulent flow, may well justify the necessary investment, as parameter ranges directly relevant to Air Force applications would then be able to be addressed in the deterministic and efficient manner described in the framework of the present research.

VI. REFERENCES

Abdessemed, N., Sherwin, S. J. and Theofilis, V. On Unstable 2D Basic States in Low Pressure Turbine Flows at Moderate Reynolds Numbers, AIAA Paper No. 2004–2541, 2004.

Abdessemed, N., Sherwin, S.J. and Theofilis, V. Floquet stability analysis of periodic states in low pressure turbine flows at moderate Reynolds numbers. Congreso de Métodos Numéricos en Ingeniería 2005, July 4-7, 2005, Granada, Spain, 2005.

Barkley, D. and Henderson, R. D. Three-dimensional Floquet stability analysis of the wake of a circular cylinder. Journal of Fluid Mechanics 322:215–241, 1996.

Briley, W. A numerical study of laminar separation bubbles using the Navier-Stokes equations. Journal of Fluid Mechanics, 47: 713-736, 1971.

Chomaz, J.-M. Global Instabilities in Spatially Developing Flows: Non-Normality and Nonlinearity, Annual Reviews of Fluid Mechanics, 37:357-392, 2005.

Collis, S. S., Joslin, R. D., Seifert, A. and Theofilis, V. Issues in active flow control: theory, control, simulation and experiment. Progress in Aerospace Sciences 40:237-289, 2004.

Crouch, J. D. On the onset of buffet on a NACA-0012 wing at an angle of attack. 3rd Global Flow Instability and Control symposium, Crete, Greece, Sept. 25 – 28, 2005.

Dallmann, U., Vollmers, H., Su, W.-H. & Zhang, H.-Q. Flow topology and tomography for vortex identification in unsteady and in three-dimensional flows. Proceedings IUTAM Symposium on Simulation and Identification of Organized Structures in Flows, Lyngby, Denmark, May 25-29, 1997.

Drazin, P. and Reid, W. 1981 Hydrodynamic stability . Cambridge University Press.

Fasel, H. F., Gross, A. and Postl, D. Control of separation for low pressure turbine blades: numerical simulations. Proc. of the Global Flow Instability and Control Symposium II (V. Theofilis, ed.) Crete, Greece, June 11-13, 2003.

Hammond D. A. and Redekopp L. G.. Local and global instability properties of separation bubbles. Eur. J. Mech. B/Fluids, 17:145–164, 1998.

Hein, S. and Theofilis, V. On instability characteristics of isolated vortices and models of trailing vortex systems. Computers and Fluids 33:741-753, 2004.

Karniadakis, G. Em. and Sherwin, S. J. Spectral/hp Element Methods for Computational Fluid Dynamics. Oxford University Press, (2nd ed.), 2005.

Morzynski, M., Afanasiev, K., Thiele, F. Lösung von großen unsymmetrischen Eigenwertproblemen bei der Stabilitätsanalyse auf der Grundlage der 2-D Navier-Stokes-Gleichungen, Institutsbericht 08/96 Hermann Föttinger-Institut für Strömungsmechanik, Technische Universität Berlin, Berlin, 1996.

Noack, B. R., Tadmor, G. and Morzynski, M. Low-Dimensional Models For Feedback Flow Control. Part I: Empirical Galerkin models. AIAA 2004-2408. 2nd AIAA Flow Control Conference, June 28-July 1, 2004, Portland, OR, USA.

Poliashenko, M. and Aidun, C.K., A Direct Method for Computation of Simple Bifurcations, J. Comp. Physics, 121 (1), 1995.

Postl, D., Gross, A. and Fasel, H. 2004 Numerical investigation of active flow control for low pressure turbine blade separation. AIAA Paper 2004-0750.

Rizzetta, D. and Visbal, M. Numerical simulation of separation control for a transitional highly-loaded Low-Pressure Turbine cascade, AIAA Paper No. 2004-2204.

Schmid, P. J and Henningson, D. S. Stability and transition in shear flows. Springer, 2001.

Simens, M., González, L., Theofilis, V. and Gómez-Blanco, R. On fundamental instability mechanisms of nominally 2-D separation bubbles. IUTAM Laminar-Turbulent Symposium VI, Bangalore, India, Dec. 13-17, 2004. (R. Narasimha and R. Govindarajan eds.) Springer 2005.

Sondergaard, R., Rivir, R., Bons, J. and Yurchenko, N., Aerodynamic and Thermal Control of Turbine and Aerodynamic Flows, AIAA Paper No. 2004-2201.

Theofilis, V. Global linear instabilities in laminar separated boundary-layer flow. IUTAM Laminar-Turbulent Transition Symposium V, Sedona AZ, USA (H. Fasel and W. Saric eds.), 663-668, Springer, 1999.

Theofilis, V. Globally-unstable flows in open cavities. AIAA Paper 2000-1965, 2000.

Theofilis, V. Advances in global linear instability of nonparallel and three-dimensional flows. Prog. Aero. Sciences, 39 (4):249–315, 2003.

Theofilis, V., Hein, S. and Dallmann U. Ch. On the origins of unsteadiness and three-dimensionality in a laminar separation bubble. Phil. Trans. Roy. Soc. London (A), 358:3229–3246, 2000.

Theofilis, V. and Sherwin, S. J. Global instability in the trailing-edge of a NACA 0012 aerofoil, 15th International Symposium on Air Breathing Engines Conference, Bangalore, India, Sept. 3-7, 2001, Paper No. ISABE 2001-1094.

Theofilis, V., Barkley, D. and Sherwin, S.J. Spectral/hp element technology for flow instability and control, Aeronautical Journal 106:619-625, 2002.

Theofilis, V., Sherwin, S.J. and Abdessemed, N. On global instabilities of separated bubble flows and their control in external and internal aerodynamics applications. NATO-RTO Symposium "Enhancement of NATO military flight vehicle performance by management of interacting boundary layer transition and separation" RTO-MP-AVT-111, Prague, Czech Republic, 4-7 October 2004.

Tuckerman, L.S. and Barkley, D. Bifurcation analysis for timesteppers. In E. Doedel and L.S. Tuckerman, editors, Numerical Methods for Bifurcation Problems and Large-Scale Dynamical Systems, 119:453-466. Springer, New York, 2000.

Wissink, G. DNS of separating, low Reynolds number flow in a turbine cascade with incoming wakes. Proc. of the Engineering Turbulence Modelling and Experiments IV, (W. Rodi and N. Fueyo, eds.), pp 731–740, Mallorca, Spain, 16-18 September 2002.

Wu, X. and Durbin, P. A. Evidence of longitudinal vortices evolved from distorted wakes in a turbine passage. Journal of Fluid Mechanics, 446:199–228, 2001.

VII. OTHER ACTIVITIES SUPPORTED BY GRANT

1. Collaborations

On account of knowledge attained in the framework of the present Grant, the following new collaborations have been started:

- Dr. S. Collis (Sandia Labs) and Dr. Alexander Fedorov (Moscow Institute of Physics and Technology) on compressible attachment-line instability.
- Prof. Rama Govindarajan (Jawarhalal Nehru Center for Advanced Scientific Research, Bangalore, India) on large-scale computations for the BiGlobal eigenvalue problem.
- Dr. Olaf Marxen (KTH, Stockholm, Sweden) on separation bubble instability, numerical methods for the BiGlobal eigenvalue problem and DNS.

Regular contacts are kept with these teams.

2. Visits/Student Exchanges

Partially supported by the Grant, Theofilis visited Imperial College in Feb. 2004 and Dec. 2005 and attended two invitation-only meetings, namely the NATO RTO AVT-111 meeting, Prague, Czech Republic, Nov. 2004, and the IUTAM Laminar-turbulent transition symposium VI, Bangalore India, Dec. 2004.

Abdessemed visited Madrid 1st through 15th of Feb. 2005

VIII. PRESENTATIONS, PUBLICATIONS AND AWARDS

1. Presentations

Fully- or partially (in addition to WOS or other funds) supported by the Grant

Theofilis delivered talks ate the following meetings:
- AFOSR Contractors' and Grantees' Meetings:
    o Destin, FL (2003),
    o Denver, CO (2004),
    o Long Beach, CA (2005)
- Invited talks:
    o UC San Diego, CA, visiting Prof. T. Bewley
    o U of Arizona, Tucson, AZ, visiting Prof. I. Wygnanski.
- AIAA contributions:
    o Portland, OR (2004)

Both Sherwin and Theofilis will deliver talks at:
- EUROMECH, European Fluid Mechanics Conference, Stockholm 2006.

Abdessemed delivered talks at:

- 13th Conference on Finite Elements for Flow Problems 2005, Swansea
- Methodos Numericos in Ingenieria 2005, Granada
- 3rd Symposium on Global Flow Instability and Control September 2005 Crete, Greece.
- AIAA San Francisco 2006 – planned.

2. Publications

Fully supported by the Grant

Theofilis, V. and Sherwin, S. J. 2003 On 2D basic states in LPT flows and their 3D instability. Minnowbrook IV Workshop on Boundary Layer Transition and Unsteady Aspects of Turbomachinery Flows. (LaGraff, J.E. and Ashpis, D.E. eds.). NASA/TM-2004-212913

Abdessemed, N., Sherwin, S.J. and Theofilis, V. On Unstable 2D Basic States in Low Pressure Turbine Flows at Moderate Reynolds Numbers. AIAA Paper 2004-2541.

Abdessemed, N., Sherwin, S.J. and Theofilis, V. Floquet stability analysis of periodic states in low pressure turbine flows at moderate Reynolds numbers. Congreso de Métodos Numéricos en Ingeniería 2005, July 4-7, 2005, Granada, Spain.

Theofilis, V., Sherwin, S.J. and Abdessemed, N. On global instabilities of separated bubble flows and their control in external and internal aerodynamics applications. NATO-RTO Symposium *"Enhancement of NATO military flight vehicle performance by management of interacting boundary layer transition and separation"* RTO-MP-AVT-111, Prague, Czech Republic, 4-7 October 2004.

Abdessemed, N., Sherwin, S.J. and Theofilis, V. Linear stability analysis of the flow past a low-pressure turbine blade. 36th AIAA Fluid Dynamics Conference and Exhibit, San Francisco, CA, June 5-8, 2006.

Abdessemed, N., Sherwin, S.J. and Theofilis, V. BiGlobal stability analysis of low-pressure turbine flows. Part I: the eigenvalue problem. (in preparation).

Abdessemed, N., Sherwin, S.J. and Theofilis, V. BiGlobal stability analysis of low-pressure turbine flows. Part II: the pseudospectrum. (in preparation).

Partially supported by the Grant

Theofilis, V., Seifert, A., Joslin, R. D., and Collis, S. S. Poster on Theoretical and Experimental Active Flow Control. AIAA Summer Meeting, Portland, OR, June 28 – July 1, 2004.

Collis, S.S., Joslin, R.D., Seifert, A. and Theofilis, V. Issues in active flow control: theory, control, simulation and experiments. Progress in Aerospace Sciences 40:237–289, 2004 **(Top25 paper - Prog. Aero. Sci.)**

Simens, M., González, L., Theofilis, V., and Gómez-Blanco, R. 2005 On fundamental instability mechanisms of nominally 2-D separation bubbles. IUTAM Laminar-Turbulent Symposium VI, Bangalore, India, Dec. 13-17, 2004. (R. Narasimha and R. Govindarajan eds.) Springer 2005.

Pitt, R.E., Sherwin, S.J. & Theofilis, V., 2005, BiGlobal stability analysis of steady flow in constricted channel geometries, Int. J. Numer. Meth. Fluids, 47:1229-235, 2005

3. Awards, Distinctions

Theofilis is the national coordinator of the 2nd Spanish Pilot Center of European Research Consortium On Flow Turbulence And Combustion (ERCOFTAC – www.ercoftac.org), based in Madrid.

Abdessemed is finalist of the ERCOFTAC (www.ercoftac.org) Osborne Reynolds Colloquium and Student Research Award, April 2006, UK.

IX. APPENDIX

The T-106/300 LPT blade geometry

The coordinates defining the surface of the T106/300 LPT blade are

Pressure side		Suction side	
x	y	x	y
0.00	0.00	-1.87	1.52
3.61	1.89	-3.14	9.76
9.21	11.69	-0.67	26.13
16.02	22.84	2.80	38.97
22.37	31.42	6.92	50.02
28.50	38.31	11.65	59.87
34.53	44.03	17.02	68.76
40.56	48.94	23.02	76.78
46.64	53.28	29.59	83.93
52.75	57.17	36.68	90.23
58.83	60.62	44.22	95.66
64.81	63.63	52.14	100.23
70.67	66.19	60.36	103.93
76.38	68.28	68.80	106.76
82.47	70.07	77.39	108.79
89.07	71.74	86.14	110.05
95.66	73.15	95.01	110.55
102.27	74.26	103.98	110.30
108.90	75.05	113.01	109.31
115.70	75.49	122.02	107.62
122.77	75.56	130.96	105.31
130.15	75.24	139.81	102.48
137.81	74.51	148.56	99.20
145.71	73.38	157.19	95.56
153.79	71.85	165.70	91.61
161.99	69.92	174.08	87.41
170.26	67.62	182.32	83.01
178.52	64.97	190.40	78.45
186.73	61.99	198.31	73.79
194.84	58.73	206.03	69.05
202.78	55.21	213.54	64.27
210.54	51.50	220.84	59.49
218.05	47.63	227.89	54.75
225.31	43.66	234.70	50.06
232.29	39.64	241.25	45.47
238.96	35.62	247.51	40.99
245.32	31.65	253.48	36.66
251.36	27.78	259.14	32.51
257.07	24.04	264.47	28.55
262.43	20.48	269.46	24.81
267.45	17.12	274.10	21.32
272.09	14.00	278.37	18.08
276.36	11.14	282.25	15.14
280.23	8.56	285.72	12.49
283.68	6.28	288.77	10.16
286.68	4.31	291.37	8.16
289.22	2.67	293.52	6.52
291.27	1.36	295.18	5.25
292.79	0.39	296.50	4.00
295.45	0.28	296.87	2.45